Grenoble INP - Phelma

Politecnico di Torino
Corso di laurea in Nanotechnologies for ICT

MAGNETIC SENSOR BASED ON MAGNETIC TUNNEL JUNCTION

Student:
TERESI Salvatore

Supervisor:
BARADUC Claire

RICCIARDI Carlo

ALLIA Paolo Maria
Eugenio Icilio

Contents

Glossary

GMR: Giant magnetic resistance
MRAM: Magnetic random acces memory
MTJ: Magnetic tunnel junction
Mumax: Program able to perform micro-magnetic simulations
RVM: Rigid vortex model
TMR: Tunnel magnetic resistance
TVM: Two vortex model

List of Figures

Tables

Introduction

Spintronics (or spin electronics) is a field of solid-state physics where the spin of the electron is used as an extra degree of freedom to control electronic transport.
The two main phenomena on which it is based, the Giant magnetoresistance (GMR)[1,2] and the tunnel magnetoresistance (TMR)[3] were demonstrated, respectively in 1988 and 1975.
At the beginning, GMR seemed to be more interesting while TMR was a weak effect working at really low temperatures (4.2 K). After some recent developments about magnetic tunnel junctions (MTJ) with very high tunnel magnetoresistance at room temperature, they started to be studied with more interest. In particular it is possible to obtain different magnetic states for the free magnetic layer. Each of them lead to important physical phenomena in MTJs that needs to be explored. Until now, a complete analysis of some of them is lacking.
For this reason, during this work, a study about MTJs was done. Hence, the main point of the work was to understand the behaviour of these devices for a specific magnetic ground state, called vortex state. This magnetic state consist of a circular in-plane magnetization with a core, in which the magnetization is out-of-plane. The shape of MTJs implemented will be cylindrical, because it was demonstrated that it is able to favour the mentioned state. The aim of this work is to study the magnetic response to an external magnetic field sweep in order to identify features able to give some advantages in memory or sensors applications [4,5,13].
Also new shapes will be introduced in the analysis and they will be explored carefully in order to optimize the qualities of MTJ based on vortex state or solve new problems and drawbacks met during the study.

The work showed in the following chapters can be divided in 3 parts: first a theoretical description of the MTJ and more specifically the magnetic state of its free layer. A second part will describe the main core of the work, showing the simulations performed and the physical models used to describe the phenomena encountered. And finally the conclusion of this work and a possible implementation in future with a PhD.

SPINTEC laboratory and research group

SPINTEC is one of the leading research laboratories in spintronics. The main focus is the study of nanomagnetism phenomena and spin-dependent electronic transport for innovative devices that could lead to possible industrial applications. The hope is to replace devices based solely on electronics with devices based on magnetism, the latter being enviromental friendly, reducing power consumption and offering through the spin of electrons another degree of freedom.

Going into the details of this work, one of the most important fields is the study of magnetic sensors. In this context, Spintec laboratory collaborates with **Crocus Technology**, a start-up company. Spintec laboratory is in charge of assessing the feasability options for sensors. In particular, it is currently studying from a physical point of view the potentials of vortex based sensors.

In this context, during the last semester I joined the two people in charge at Spintec for studying vortex sensors: Claire Baraduc and Salim Dounia. Salim Dounia is a PhD student hired by Crocus Technology in collaboration with Spintec, while Claire Baraduc is supervising the work and is also the contact point between the company and the laboratory.

Chapter 1

The magnetic tunnel junction (MTJ) and the magnetic vortex state

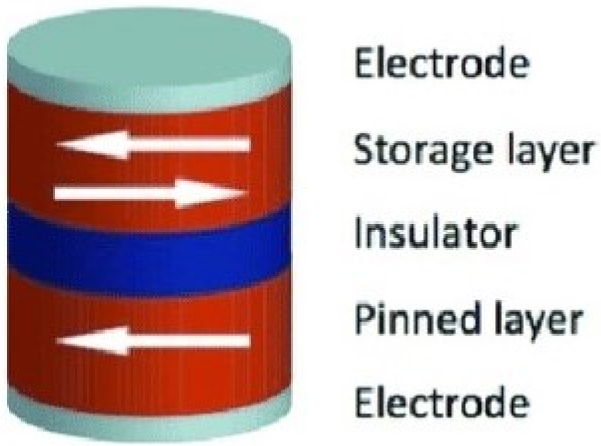

Figure 1.1: Schematic illustration of a magnetic tunnel junction[22].

This chapter will present a theoretical explanation of the electronic transport in magnetic tunnel junction (MTJ), i.e. the physical concept of magnetoresistance. Then the magnetic state studied, the vortex state, will be introduced with a theoretical discussion on competing energies to explain its existence. The conclusion will give a first approach to magnetic tunnel junctions in vortex state, that are the subject of the thesis, and the main argument of the next chapter.

1.1 MTJ's theoretical principle

A spintronics device is a structure made of two ferromagnetic layers, separated with a layer of non-ferromagnetic material with the thickness of all layers in the nanometric range. There are two types of spintronics magnetoresistances depending on the conductive nature of the non-ferromagnetic layer. When this layer is a conductor, the basic working principle is the giant magnetoresistance (GMR), while as in the case of the devices studied during this work, and presented in fig. 1.1 when there is a thin insulator layer, the physical phenomenon is the tunnel magnetoresistance (TMR).
Furthermore, one of the ferromagnetic layers has a fixed magnetization (it is called "pinned layer") while the other's magnetization can rotate and align along the external magnetic field (defined as "sense layer"). Interestingly, the relative magnetization orientation between the two ferromagnetic layers allows a larger or lower amount of current to pass through the device going from a contact to the other (through tunneling when an insulating layer in used). In this way, by setting a proper orientation for the magnetization of pinned and free layer it is possible to regulate the amount of current that is allowed to tunnel through the insulating layer, hence passing from one electrode to the other. This is the reason why it is called magnetoresistance.
The reason why more or less current is allowed to pass as a function of the relative magnetization orientation is related to the spin direction that every electron intrinsically has. This establishes which and how many electrons are allowed to flow (independently from the thickness of the insulating layer that is fixed for the different magnetizations configurations and reduce the net amount of electron flow).

1.1.1 Magnetoresistance

From literature different magnetoresistive effect were discovered during the years: **the giant magnetoresistance (GMR)** when the non-ferromagnetic material that separates the two ferromagnetic layers is a conductive layer; and **the tunnel magnetoresistance (TMR)** specific for MTJs having an insulator barrier between two ferromagnetic layers.
The TMR has recently attracted much interest because of the use of some alloys and insulating layers (like MgO) allowing a large TMR at room temperature[15,16] while at the beginning it was not considered for applications and GMR was predominating.

The physics at the basis of the current behaviour is easily explained. Assuming a parallel magnetization for both ferromagnetic layers, the band structure for the two ferromagnetic layers is represented in the following way (fig. 1.2):

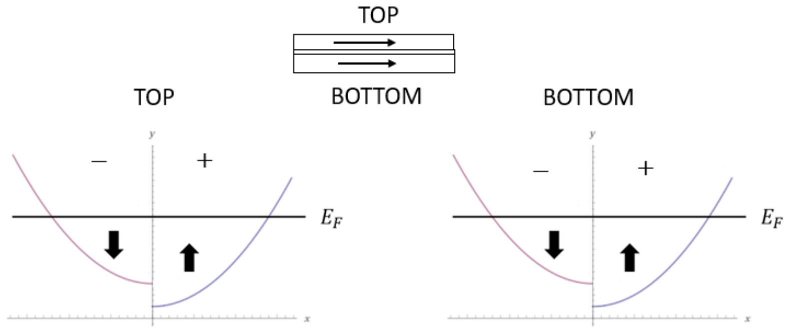

Figure 1.2: Schematic illustration of the band structure for top and bottom layers in case of parallel magnetization. E_F is the Fermi energy for this system.

Due to the presence of a magnetization, electrons have a favoured spin hence a lower energy in the system. The current flows through tunnelling from the top to bottom layer, with the rule of conserving the spin while tunnelling. Hence the conductivity for parallel magnetization case is:

$$G_P \propto n_{\{top,+\}} n_{\{bottom,+\}} + n_{\{top,-\}} n_{\{bottom,-\}} \tag{1.1}$$

obtained by the Fermi golden rule. n represents the density of electrons states at Fermi level in the band structure. When the index is *top*, n defines the density of states in the top layer, at Fermi energy. While the index *bottom* defines the density of states in the bottom layer at Fermi energy. $+$ and $-$ are used to identify the majority and minority electron spins into the two layers. Hence the system shows a high conductivity due to the large contribution of the first term. Instead the physical representation of the states for anti parallel layers is the following (fig. 1.3):

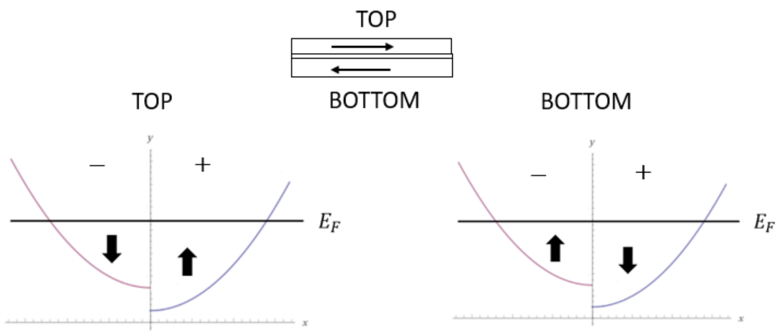

Figure 1.3: Schematic illustration of the band structure for top and bottom layers in case of anti-parallel magnetization. E_F is the Fermi energy for this system.

Again due to the presence of a given magnetization, electrons have a favoured spin. The current flows through tunnelling from the top to bottom layer, hence the conductivity for anti parallel magnetization case is:

$$G_{AP} \propto n_{\{top,+\}} n_{\{bottom,-\}} + n_{\{top,-\}} n_{\{bottom,+\}} \tag{1.2}$$

with the same explanation as for the parallel conductivity. This time both terms give the same contribution to the total conductivity, that is much lower than the previous one. This explains the large resistance difference between the two cases.

For this reason, two different states can be identified similarly to a logic '0' and '1' and used for memory applications (MRAM). On the other hand magnetic tunnel junctions can also be used as magnetic field sensors since the magnetization of one layer is free to rotate under applied field whereas the magnetization of the other layer is pinned: the value of the resistance is thus directly related to the magnetic field.

1.1.2 MTJ with vortex state

The vortex state magnetization consists of a core with an out of plane magnetization around of which magnetic moments are organized in a circular in-plane magnetization (see fig. 1.4). This kind of configuration can be the favoured at remanence for a free layer with specific dimensions. This state naturally allows to have a magnetization that grows linearly as a function of the external applied field. This linear response is very interesting for sensors; by contrast, sensors based on single domain MTJs are more complex devices since they require a perpendicular magnetic field bias produced by permanent magnets. The vortex state gives the possibility to see a progressive change of the magnetization when an external magnetic field is applied to the sense layer.

The great advantage is linked to the ability to check the presence of a vortex state in a layer through the study of the magnetoresistance. That overcomes the problem of magnetic measurements that typically need a large amount of magnetic materials.

For a vortex state in a circular layer, at zero external applied field, the total in-plane magnetization is null (see fig. 1.4). In fact the vortex's core is placed at the center of the circle, hence for symmetry there are no parts predominating over each other:

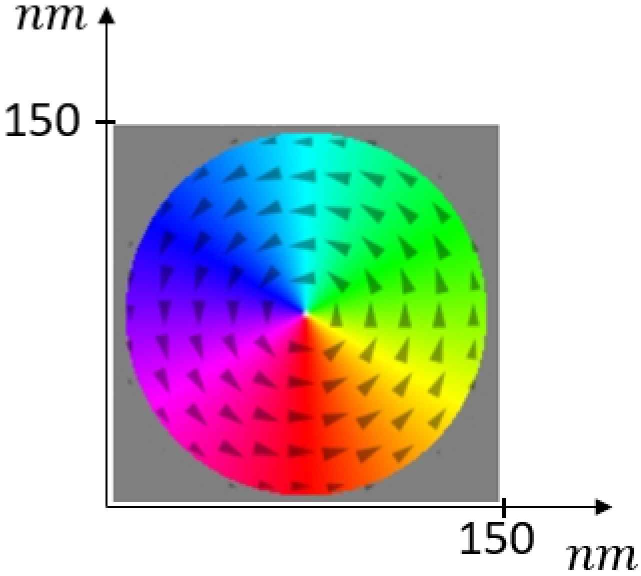

Figure 1.4: Vortex state configuration showed through a micromagnetic simulation of a circular layer at zero magnetic field.

The core is at the center (white point at the center of the circle), and the curling magnetization is equally spaced all around leading ideally to no magnetic surface charges at the edges (since magnetization remains tangent to the edges).

When an external field is applied to this system, the vortex shifts in a direction perpendicular to the field orientation, resulting in a magnetic configuration that is no longer symmetric.

By gradually increasing the external field, the number of magnetic moments in the dot with the same direction as the field increase also gradually, while doing so, the core is shifted more and more toward the edge far from the center (figg. 1.5 *b* and *d*). At a certain point, the core goes out (later it will be explained that this point is called annihilation field) and magnetization is uniform within the dot (figg. 1.5 *a* and *e*).

The term *dot* will be used from now on to define a magnetic material with the shape of a circle or an ellipse (or a portion of it).

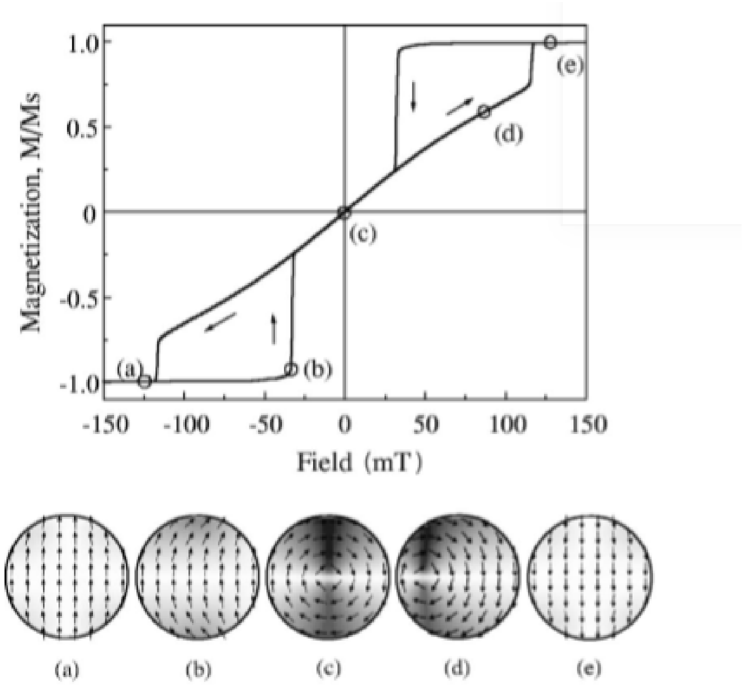

Figure 1.5: Hysteresis cycle obtained for a circular layer having a vortex state as a ground energy state when the magnetization is plotted as a function of the external applied magnetic field[6].

The more parallel (antiparallel) the magnetization of the free layer is with respect to the pinned one's where the magnetization is fixed, the smaller (larger) will be the resistance. From the picture above (fig. 1.5) it is possible to see the evolution of the vortex state under an applied field. Between figures (d) and (e) the vortex has gone out of the system; the corresponding magnetic field is defined as **annihilation field**; also another interesting fact is the ability to re-nucleate the vortex state at an applied field larger than zero while reducing the field value starting from a from positive external applied field (from picture (e) to (c)). The field at which the vortex state is recovered is called **nucleation field**.

1.2 State of art

The reason why it is interesting to study MTJ's based on vortex state lies in the potentiality to have a system with a linear response with the advantage of having a much easier technological processes during fabrication. In fact, most of electronic devices based on MTJ were built with a single domain state for the free layer. But in this configuration it is possible to have a linear response only if the magnetizations of the two layers are perpendicular (as showed in fig. 1.6).

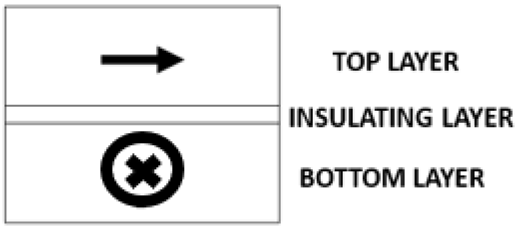

Figure 1.6: Graphical illustration of the direction of the magnetization for a MTJ for the pinned layer (bottom) and the free layer (top). The magnetization directions for the two layers are perpendicular and in-plane.

From the point of view of the fabrication process, a MTJ with the magnetization as shown in fig. 1.6 is not easy to build. In fact, in order to have the two magnetization fixed and perpendicular it is necessary either to develop complex material engineering (with multiple annealing steps under field), or to add permanent magnets.

Furthermore, in a rectangular layer, a magnetization orientation is favoured while the other orientation is less stable. These two orientations are respectively directed towards the longer and shorter sides of the rectangle and are respectively called **easy axis** and **hard axis**.
Hence it is important to control the anisotropy of the layer that depends on the geometry but also on the material used for the magnetic layer.

1.3 Energy study of the vortex state

It can be shown that in a certain range of parameters for a cylindrical layer the lowest energy magnetic state is the vortex one at the expenses of the single-domain one (fig. 1.7):

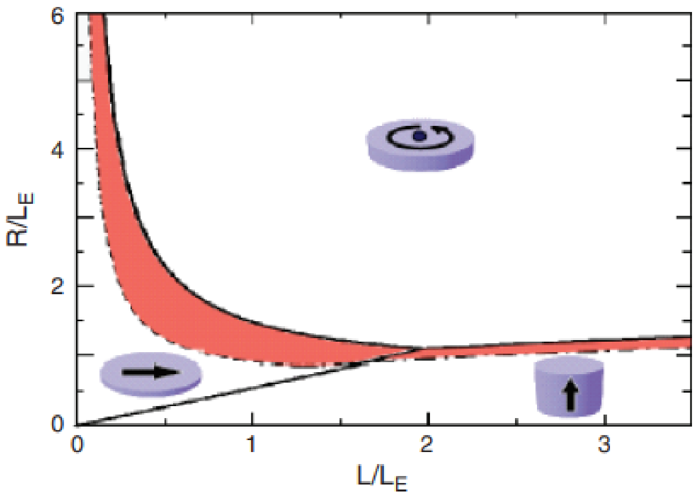

Figure 1.7: Graph showing the ground energy states for cylindrical magnetic layers as a function of layer's dimensions where R is the radius and L the thickness, both normalized by the exchange length. There are 3 different possible states: two are single domain states, respectively in-plane and out-of-plane and the last one is the vortex state[6].

In the figure shown, L represent the thickness of the free layer, R is the radius of the layer and L_E is the exchange length of the layer; L_E depends on the magnetic properties specific of the material as the exchange stiffness A_{ex} and the saturation magnetization M_s. The exchange length is $L_E = \sqrt{\frac{A_{ex}}{K}}$ where K is the anisotropy constant. The black line represents the cross energy point between vortex and single domain states, while the color region correspond to metastable vortex.

By respecting the dimensional rules extrapolated from this graph for the thickness and the radius of the free layer, it is possible to always have a vortex state for the magnetization, being the ground state energy for the system.
The vortex state regions include a variety of combinations of radii and thicknesses, hence it will be important to see also which combination shows the best physical properties for this state.

1.3.1 Nucleation and Annihilation fields

The hysteresis cycle (fig. 1.5) will be discussed by considering the energy associated to the magnetic states, and more specifically the two phenomena called *nucleation* and *annihilation*. The nucleation field is by definition the point of the hysteresis curve at which a vortex is created in the magnetic disk. On the contrary, when a vortex state is already the ground state of the layer, the annihilation field can be defined, as the field at which the vortex core goes out of the dot, hence causing a single-domain state to appear.

A change of magnetic state is associated with a new energetic ground state. So in order to understand why and how annihilation and nucleation take place, a theoretical analysis of the competition between different energies is required. For a magnetic disk, it was demonstrated [6,20] that the energies that play a role are: the magnetostatic energy (E_{ms}), the Zeeman energy (E_z) and the exchange energy (E_{exch}).
First it is imperative to specify that the energies are often normalized to the volume: in this case the energy density is defined through the capital letter W. A stronger normalization is performed by dividing by the volume and by the volumic demagnetizing energy $1/2\mu_0 M_s^2$. In this case the symbol for this normalized energy is w and it has no unit, by contrast to W expressed in J/m^3.
These notations, W and w, are chosen in reference to Guslienko's paper [6].
Now it will be given a closer description of the energy terms mentioned in the previous paragraph:

The magneto-static energy is a factor that accounts for the interactions between the magnetic moments composing the layer and the field they cause inside the layer. The theoretical formula used to account for this energy is (eq. 1.3):

$$E_{ms} = \frac{1}{2}\int dS \int dS' \frac{\sigma(r)\sigma'(r')}{(r - r')} \tag{1.3}$$

where S and S' account for the lateral surface of the cylindrical free layer; σ and σ' are the surface charges generated by the magnetic moments that are not tangent to the side surface; r and r' are the position of these interacting charges with respect to a reference system.
The surface charges are themselves function of the relative core displacement s along x-axis and the angle (θ) at which they are placed with respect to the x-axis (eq 1.4):

$$\sigma(\mathbf{r}) = -M_s \frac{s\sin(\theta)}{\sqrt{1 + s^2 - 2s\cos(\theta)}} \tag{1.4}$$

At the end, a simple formula for the magnetostatic energy can be shown after solving and simplifying the formula showed previously (eq. 1.3, normalized with respect to the volume and the saturation magnetization) (eq. 1.5):

$$w_{ms}(s) = w_{ms}(0) + \frac{\beta s^2}{2\pi} \times N(s, \beta) \tag{1.5}$$

where $w_{ms}(0)$ is the normalized magnetostatic energy for the case in which there is no core displacement (no external applied field). Ignoring the charges on the top surface generated by the core, this quantity is zero. β is the ratio between thickness and radius L/R, s is the vortex relative displacement x/R where x is the vortex core displacement and $N(s, \beta)$ is a complex factor including a 3D integral that is called demagnetizing factor.

The Zeeman energy is due to the presence of a external magnetic field and described by the following formula (eq. 1.6):

$$E_z(s) = -\int_V d^3\mathbf{z}\mathbf{M(z)}\mathbf{H} \tag{1.6}$$

where $M(z)$ is the volume magnetization of the layer, and H the external applied field. By developing the integral, it can be written into an easier but approximated way as (eq. 1.7):

$$w_z(s) = -h(s + O(s^3)) \tag{1.7}$$

for small vortex displacements; where h is the normalized applied field equal to $\frac{H}{M_s}$, and s is the displacement of the vortex core with respect to the equilibrium position at zero field normalized by the disk radius.

The exchange energy takes into account the energy cost of non collinear adjacent moments. In fact in the case of a curling magnetisation for the vortex state, neighbouring sites have different moments and thus a high value of the exchange term. It is defined mathematically as:

$$E_{exch} = \frac{A}{2} \int d^3\mathbf{r} \sum_{\alpha} (\nabla m_\alpha)^2 \tag{1.8}$$

where A is the exchange stiffness, while m is the normalized magnetization and $\mathbf{r}$ is the 3D position vector and α identify the different magnetic moments of the magnetic material.

The exchange energy of the shifted vortex can be written as follows for small relative displacement of the vortex core (eq. 1.9):

$$w_{exch}(s) = w_{exch}(0) - \frac{1}{2}(\frac{L_E}{R})s^2 \qquad (for \quad s \to 0) \tag{1.9}$$

where $w_{exch}(0)$ account for the exchange energy where no external field is applied and hence the vortex is placed at the center of the circular layer; s is the relative core displacement, L_E is the exchange length.

These energy factors depend on the magnetic state and the external applied field, hence while applying a field, some of them grow while other decrease. For example for Zeeman energy, being negative, the more the core is shifted (hence the field applied is higher) and the lower will be the energy required for the final state with respect to the original position for zero field.
Similarly for the exchange energy that has a smaller energy for the shifted core because of a smaller region in which the magnetization is perfectly circular. The ideal case for the exchange term is when the core goes out, obtaining a single domain state where all the moments are aligned and the term goes to zero.
On the contrary to displace the vortex core has a cost in magnetostatic energy with respect to the equilibrium position at zero field. In fact with a circular magnetization and no field applied, the total magnetization of the layer is null, hence no field generated from the structure can interact with the magnetic moments of the layer. So the magnetostatic energy is zero whereas the exchange energy is large. For thick disks with large radius, the vortex state is the low energy configuration.
While for a single domain, the magnetization is the largest, leading to the highest magnetostatic term possible but zero exchange energy.
So to conclude, if a vortex state is the ground for a cylindrical layer, when the external field increases at a certain point it will be energetically convenient for the system to switch from a vortex state to a single-domain one. This field is called annihilation field.
In fact in a single domain state, all the neighbouring sites have the same magnetic moment, hence the term accounting for the exchange energy is null, also the Zeeman factor is low due to the agreement of the external applied field and layer's magnetization directions.
Similarly, when decreasing the field starting from a single-domain state, at a certain point a vortex core appears at the edge of the layer and moves toward the disk center when the field is decreased to zero. In this case, the negative Zeeman energy goes to zero when lowering the external field. The magnetostatic energy is fixed and high for a single domain state and it falls to zero (no surface charges at all) when the vortex core is at the center of the disk.

1.3.2 Vortex properties

As said in the previous sections, one important phenomenon is the nucleation, hence the creation of a vortex state, starting from a single domain's one. But the process of nucleation can give different types of vortex, in particular there are two parameters that can be defined, resulting in the possibility to have up to 4 different vortices. These two parameters are:

- The circularity (or chirality)
- The polarity

they are respectively defined as: "the type of rotation for the in-plane magnetization" and "the direction at which the out of plane magnetization of the core is pointing at". While for this work the sign of the vortex core magnetization is of no interest (it will be explained later the reason), not affecting the quality or in general the feature of MTJs, the circularity needs a closer analysis.

Here two simulations for the same MTJ, having the two possible circularities (fig. 1.8):

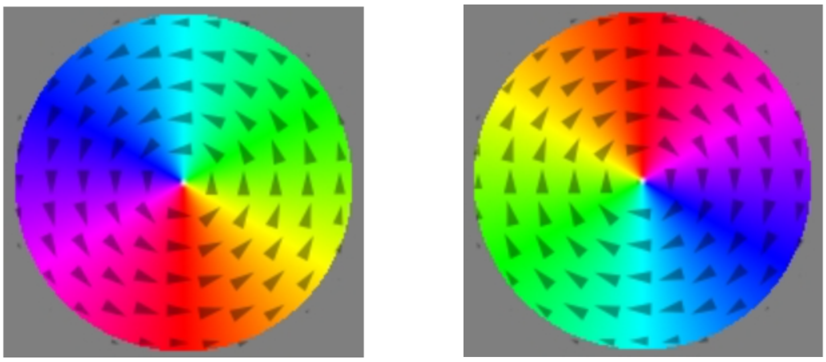

a) Vortex state in dot with counterclock-wise magnetization circularity.

b) Vortex state in dot with clock-wise magnetization circularity.

Figure 1.8: Figures obtained from micromagnetic simulations for a circle with a vortex state. The figure shows the two possible configurations for the circularity for this magnetic states. They are taken for an external field equal to zero.

During the vortex formation it is possible to distinguish between two possible and different direction of the curling magnetization. These two different chiralities of the in plane magnetization can be defined as clockwise and counterclockwise (CW and CCW respectively) while in literature to this parameter it is associated the factor C. They can also be identified by associating to them a different value like -1 for

CW and +1 for CCW.
Furthermore also the out of plane magnetization could assume two different direction, respectively pointing up or down that in literature are associated with a parameter p called polarization equal to +1 or -1 respectively.
So in total there a 4 possible configurations (see fig 1.9):

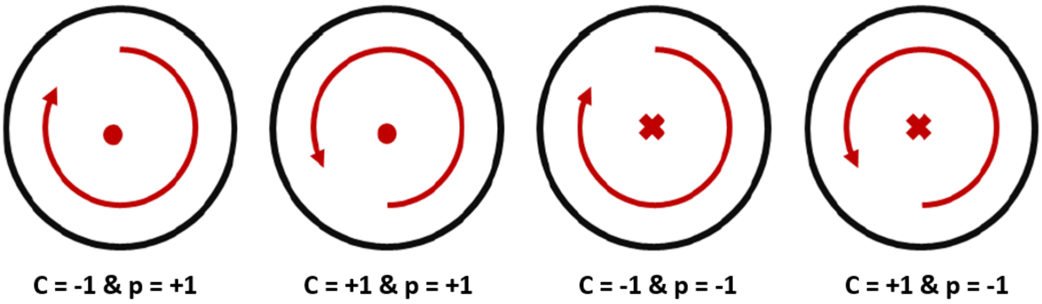

Figure 1.9: All the possible type of vortex by considering the combinations of the p and C parameters. (Courtesy of Salim Dounia)

It is important to note that the circularity determines the vortex core motion for a given external field. The vortex core moves perpendicularly to the field, either in one direction or in the other as a function of the circularity C. What is problematic is the inability to predict the vortex chirality and therefore the direction of motion of the vortex core when magnetic field is applied. From a physical point of view, it will be interesting to find a way to predict and control the circularity. To this purpose, the work of Agramunt was taken into account [9].

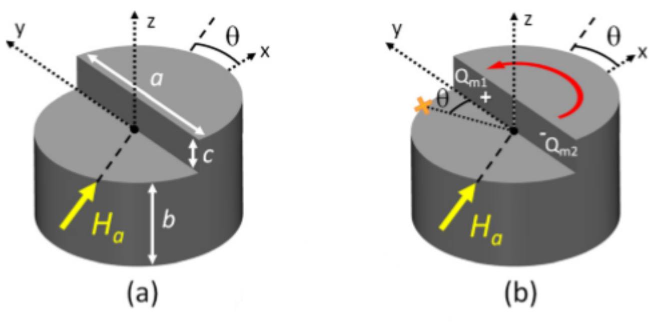

Figure 1.10: Disk representation with given dimensions. (a) Two different thicknesses are appreciated along z direction. The cut is at the half of the circle. (b) The orange cross represent the nucleation point, H_a is the direction of the external applied field. Q_{m1} and Q_{m2} are the magnetic charges generated by the field[9].

It states that a way to control this parameter is possible by the introduction of an asymmetry into the disk. In particular, as it is appreciated in fig 1.10, the asymmetry is introduced through in the disk by removing part of it.

When an external field is applied as H_a in the figure, it is possible to represent two magnetic charges as in fig. 1.10 (b). The orange cross represent the point where the vortex state nucleates associated to the direction of the external applied field. Being closer to the positive charge, the polarity will be negative. At the same time, for this type combination of cut and field applied, the circularity will be counter clock-wise (CCW).
In conclusion, it is possible to predict both polarity and circularity with a cut.
A graph summarize the circularity and polarity obtained as a function of the angle at which the field is applied (in fig. 1.11) for the previous figure 1.10.

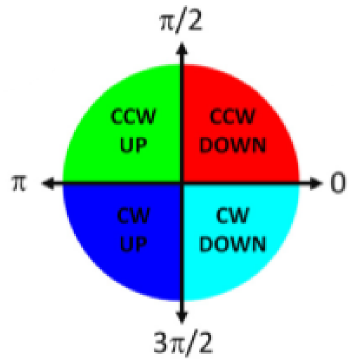

Figure 1.11: Graph showing the circularity and polarity as a function of the angle with respect to the x-axis for the applied field[9].

It is interesting to notice that there are some angles at which one of the two parameters can't be predicted. For $\pi/2$ and $3\pi/2$ the polarity can be either up or down, while for 0 and π the chirality can assume both values.

At the end, it is possible to state two rules to generalize what found for polarity and circularity:

- The resulting **chirality** depends on the position of the interface between the two thicknesses and the direction of the external applied field.
- The vortex core **polarity** depends on the sign of nearest magnetic charges to the nucleation point (orange cross in fig. 1.10). Charge sign and vortex core orientation are opposed, hence for positive (negative) charge the polarity is negative (positive).

1.3.3 Model proposed from literature

In past years a lot of models where proposed in order to describe the core motion under applied magnetic field until annihilation. Even if no one is able to reproduce all the features of this new magnetic state, they are used to evaluate with precision some important quantities.
One of the most famous is the Rigid Vortex model (RVM) proposed by *Guslienko et al.* [10] based on the work of *Usov & Peschannyj* [11], it is a simple concept but very powerful; it states that it is possible to think of the vortex moving inside the dot by recreating a circular magnetization starting from the new core position.
There is a rough approximation to ignore the edges and their relative influence into the alignement of the moments around the vortex core. But it can be used to describe with good precision small displacement of the vortex core i.e. the magnetic susceptibility at low field.

Another model often used is the two vortex model (TVM) that suppose the presence of a second vortex outside the dot. Also this second vortex has an influence on the global response of the vortex to applied field and was used to assess the influence of geometrical dimensions. The two vortex model can be used to correctly predict the vortex core dynamics at low field.

Finally, this chapter has given a theoretical introduction to the device and the phenomena studied, starting historically from the discovery of the magnetoresistive effect. Then the vortex state was introduced, which is at the center of this work with its interesting physical properties. The energy demonstration of its existence has been presented, together with some important literature on which will be based the micromagnetic simulations performed in the next chapter.

Chapter 2

Internship's main work: Micromagnetic simulations and mathematical models

The program used to run the simulations performed during my internship is Mumax[12], a free source program able to perform 3D micro-magnetic simulations, enhanced using the graphic cards of the computer to perform calculations in parallel. Specifically Cuda cores are needed, hence limiting its use to computers having a Nvidia graphic card. The advantage is the ability to have a multi-core performance that gives the results in less time respect the CPU alone. The program solves the LLG (Landau-Lifshitz-Gilbert) equations for a magnetic structure, giving an idea of the behaviour of magnetic materials.
This equation (2.1) gives the evolution of magnetization with time when subjected to a magnetic field[14]. The first term corresponds to the torque exerted by the magnetic field and the second to the damping.

$$\frac{d\vec{M}}{dt} = -\gamma\vec{M} \times \vec{H} - \lambda\vec{M} \times (\vec{M} \times \vec{H}) \tag{2.1}$$

where $\vec{M}$ is the total magnetization, t is the time interval, H is an external applied field, γ is the gyromagnetic ratio,λ is a damping parameter equal to $\alpha\frac{\gamma}{M_s}$, where α is the damping factor.
On the website there are some examples and explanations to approach to magnetic simulations. Some of them were used to perform the simulations of this work.

The main work during this internship was centered on simulations with the program mentioned. In particular four arguments are the main subjects of this work:

- Behaviour of isolated magnetic disks
- Advantages of elliptical dots
- Dot pairs interaction
- Vortex core position for non-circular dots

While for the first three, the analytical work at the basis is well-established and they just need further confirmation with the help of simulations, for the fourth subject, a different approach is performed working in the field of the hypothesis. Hence both the models proposed and the simulations performed are just trials in order to understand the phenomenon.

2.1 Isolated dots

In this section a closer analysis of isolated dots is shown. In particular the aim is to understand what happens in a system with a vortex state, by looking at the results of micromagnetic simulations. As already mentioned, three characteristics are important to study: the nucleation field, the annihilation field and in general the hysteresis curve (magnetization vs field).

2.1.1 Hysteresis loop of circular dots

Starting with the simplest case, a full circle with a vortex state was simulated. The idea is to recover the well-known hysteresis cycle by studying the magnetization as a function of the external applied field. Here the hysteresis curve obtained (fig. 2.1):

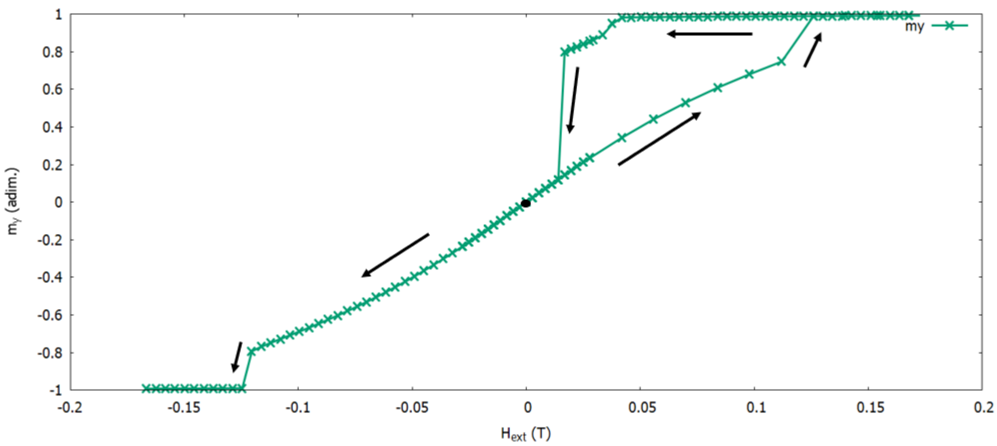

Figure 2.1: Part of an hysteresis curve of a magnetic disk (125 nm radius, 33 nm thickness) made of $NiFe$ obtained by micromagnetic simulations for a field applied along the y direction. It shows the process of annihilation and subsequent nucleation for positive magnetic fields, and only the annihilation for negative fields, giving a complete view of the linear range.

m_y is the magnetization along y direction normalized with respect to the saturation magnetization M_s, while the external applied field H_{ext} is also applied along y-axis. A linear curve can be appreciated with a jump at high field that corresponds to vortex annihilation and transition to the single domain state. Another jump is associated around zero field with the nucleation. Another important thing to notice is the small jump followed by a linear evolution of magnetization while decreasing field from annihilation to nucleation. This small jump (around 0 and 0.05 T) corresponds to another magnetic state defined in literature as S state because the configuration of the local moments within the dot resembles the letter S[18].

2.1.2 Nucleation issue and new shape for control it

One of the most important drawbacks (as anticipated in the previous chapter 1.2.2) of this system is the inability to control the vortex circularity at nucleation within a cylindrical dot.

A possible solution previously found by my research team, and based on the paper [9] is studied. Differently from [9] (look also fig 1.10), some simulations were performed with a cut that lies all along the disk thickness. This demonstrates also for this structure the validity of the conclusions in [9]. So the geometrical asymmetry is a flat into the system (fig. 2.2). In such way the circularity is controlled since nucleation always happens at the flat side of the dot.

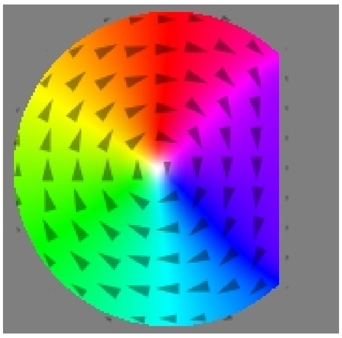

Figure 2.2: Figure showing a micromagnetic simulation's result of a circle with flat. The picture is taken for an external field equal to zero. The figure shows a clockwise circularity; it was obtained by decreasing the field starting from positive annihilation field.

Nevertheless for a problem solved, others appear, and need to be corrected. As already mentioned, the presence of a flat causes the system to be no more symmetric; one of the first and straightforward problems is the presence of a residual magnetization at remanence (hence for zero external applied field the net magnetization is non-null). The reason of this remanence magnetization can be explained by looking at the in-plane curling magnetization for this asymmetric structure. In fact, roughly speaking, having a cut in the system causes to have a region on the opposite site with respect to the center of the circle that it is not compensated. As a consequence, the vortex is shifted with respect to the center of the original circle. In order to quantify the residual magnetization, some simulations were performed with the type of cut showed in fig. 2.2.

What immediately catches the eyes is the adaptation of the circular magnetization in this new kind of structure. It causes a shift of the core from the center of the circle away from the position of the cut.

It is interesting to study the behaviour of nucleation and annihilation fields due to the shape change. To fulfill this aim, it is possible to compare the hysteresis cycle for two dots of the same size, one having the cut while the other not (as in fig. 2.3):

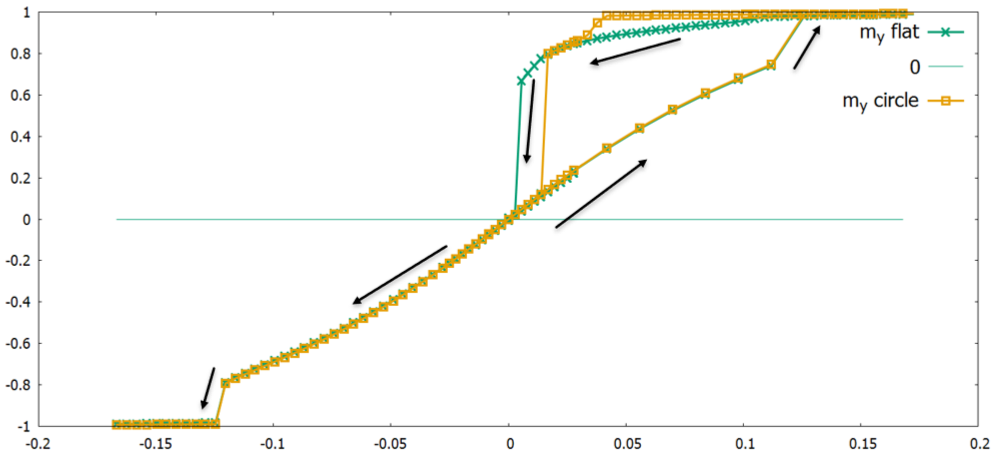

Figure 2.3: Comparison between two hysteresis loop as the one showed in fig 2.1, for magnetic disks (125 nm radius, 33 nm thickness) made of $NiFe$. One shows the results for a full circle (orange squares), the other shows the results for the same dot but with a flat (green crosses) where the penetration coefficient is $p = 30\%$. It is also possible to identify the different nucleation and annihilation fields, and the remanence magnetization at zero external applied field.

These hysteresis curves show clear reduction of the nucleation field for a flat disk compared to a circular disk. However, the behaviour at remanence and near annihilation field do not seem to differ (or at least the differences between graphs cannot be appreciated here).

For this reason we show a zoom at remanence (fig. 2.4) and a table that indicates the most important quantities evaluated (2.1).

Field Comparison between full circle and flat			
	Nucleation field (mT)	Annihilation field (mT)	Remanence (in %)
FULL CIRCLE	17	112	0
FLAT	6	112	-0,59

Table 2.1: Comparisons between annihilation and nucleation fields and the remanence magnetization for a full circle vs a circle with a flat

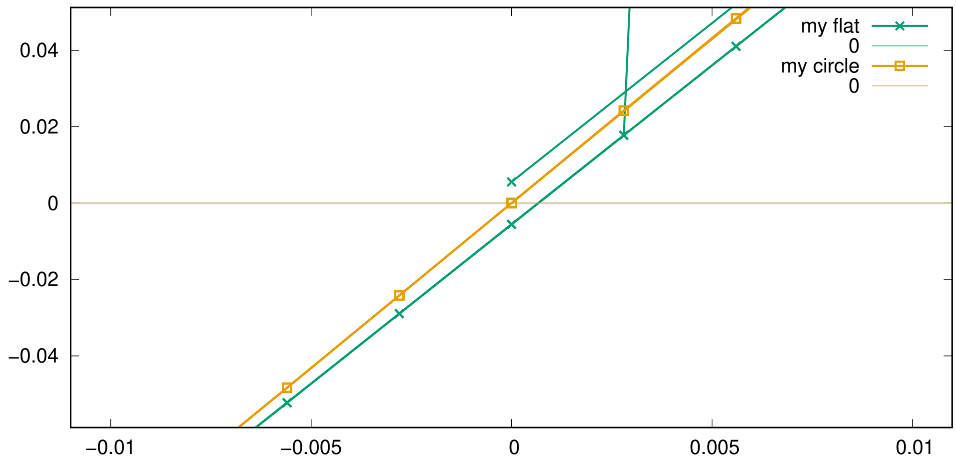

Figure 2.4: Zoom of the previous figure around zero field.

This graph (together with the associated values in the table) clearly shows that the magnetization is not zero when the external applied field is null, due to the presence of the asymmetry in the system. This lead to the mentioned remanence magnetization. Furthermore, another important fact is that the cut causes hysteresis in the linear region as showed by the splitting of the curve for the flat case (green crosses).

It is possible to conclude that the annihilation field for the two disks is the same, while the vortex nucleates at lower field, and a remanence magnetization appears at zero external applied field for flat disk.
As mentioned the creation of a remanence magnetization for zero applied field is a drawback, because of the shifting of the linear curve from zero.
Also a lower nucleation field could be a drawback, but it was not taken into account during this work.

A possible solution will be presented in the following sections (section 2.3), after the implementation of a study about the effect of interacting dot pairs.

2.2 Advantages of elliptical dots

2.2.1 Circle and ellipse

Another problem of circular dots is the dependence found between the susceptibility and the annihilation fields. The susceptibility is defined as the slope of the linear part of the hysteresis curve, hence the relative shift of the magnetization as a function of the external applied field.

$$\chi = \frac{dm}{dh} \tag{2.2}$$

For circular dots, susceptibility and annihilation field are inversely proportional, meaning that increasing the annihilation field, means to reduce the susceptibility (the slope) of the curve and vice versa. Thus, a trade off must be found between these two quantities.

This problem was already solved previously by my research team by using, instead of circular dots, elliptically shaped ones. In particular it was demonstrated that for external fields applied along the y axis (perpendicular to the one used in previous simulations), it is possible to enhance simultaneously both susceptibility and the annihilation field (see fig. 2.5):

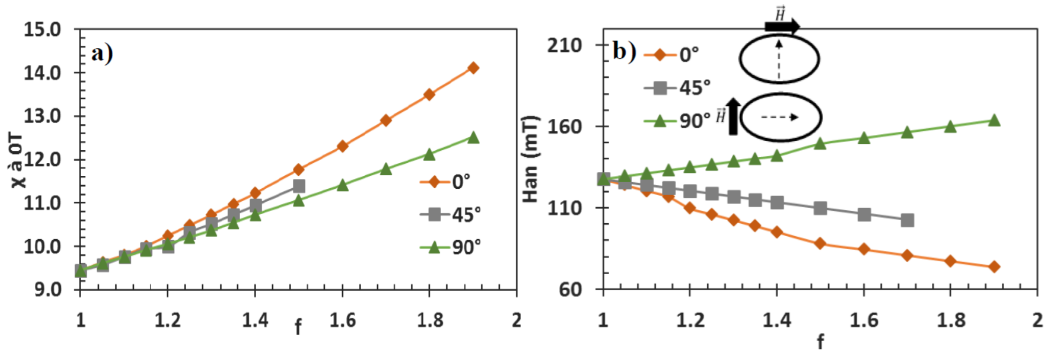

Figure 2.5: (a) Graph showing the susceptibility $\chi(0)$ as a function of the form factor $f = b/a$ in an ellipse for three different angles of the applied external field. (b) Graph showing the behaviour of the annihilation field H_{an} as function of the form factor f in an ellipse for three different angles of the applied external field. The angle are defined as follows: green triangles for 90°, grey squares for 45° and orange diamonds for 0°. (Courtesy of Salim Dounia)

From these two graphs it is possible to see that for an external applied field H along the vertical direction, the annihilation field grows together with the susceptibility. More generally, by using intermediate angles (as 45°), it is possible to reduce the inverse proportionality between these two quantities (differently from what found in circles).

Now an analysis of the results will be performed, by studying the hysteresis loop for ellipses. But first the use of ellipses requires a further study from a mathematical point of view to understand the results found by simulations.
An ellipse has the edges that change as a function of the angle, leading to some difficulties in the study of the annihilation field. This is also demonstrated by the fact that when annihilating along the x or y direction, the annihilation field found for the two cases, for the same ellipse is different.

When changing the angle, not only the annihilation field but all of the important quantities mentioned when talking about vortex state change. A complete study of the elliptically shaped dot is out of the scope of this work. A work more detailed was performed by my research team, and a doctoral chapter was written on this argument.

2.2.2 Simulations of ellipse

During the internship is studied the annihilation field for different ellipses in order to confirm the hypothesis this field only depends on the curvature's radius of the position in the ellipse where the vortex core is annihilated. This hypothesis turned out to be valid for angles like 0° and 90°. So this work was done in order to extend and generalize this result for each angle in the ellipse. From a practical point of view simulations were performed with external applied field directed towards 30° and 60° with respect to x direction.

Here is a picture (fig. 2.6), that gives a better view of the angles and the directions of the applied field and vortex core motion.

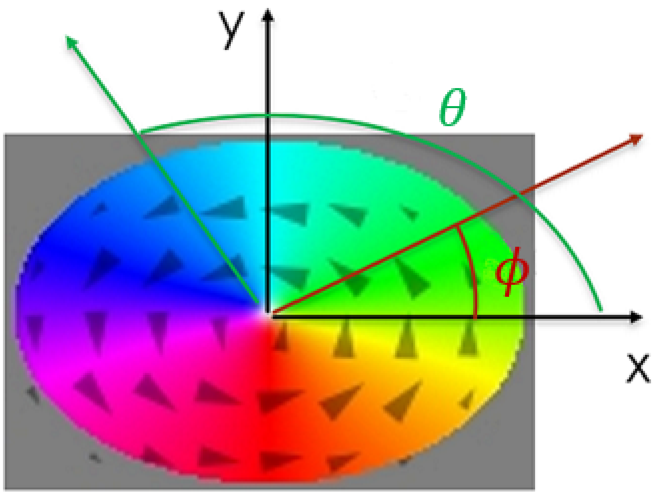

Figure 2.6: Ellipse drawing used to understand the relation between the vortex core motion (in green, angle θ) and the external applied field (in dark red, angle ϕ).

the dark red vector (angle ϕ) describes a possible random direction for an applied external field, the vector in green (angle θ) represents the direction of motion of the vortex core from the center to the edges until annihilation for the mentioned external field orientation. In fact the two vectors are perpendicular and it holds that $\theta = \phi + \pi/2$.

Going back again into the core of the work, what it is already known is the dependence in circles between the radius and the annihilation field at which the vortex disappears (as found by Guslienko [10]). But as already mentioned, for ellipses there is not a single radius but a formula to describe the curvature radius at each point of the ellipse edge.
The following equation found during the study of the curvature's radius[23] demonstrate what told earlier, linking this quantity to the angle Θ shown in fig. 2.6:

$$R_c(\theta) = \frac{b}{f}\left(\frac{1 + f^4 tan^2(\theta)}{1 + f^2 tan^2(\theta)}\right)^{\frac{3}{2}} \tag{2.3}$$

where b is the semi-small axis dimension, f is the form factor defined also as the ratio between the two dimensions of the ellipse a and b , and finally θ is the angle at which the vortex core escape from the layer. That is by definition, shifted with respect to the external applied field of 90°.

In this way it was possible to find different ellipses at which for a given angle, the curvature's radius is fixed. For example here two tables with the values used to create and simulate ellipses for the two different angles mentioned (30° and 60°) by using the equation 2.1:

30° case			
$R_c(nm)$	f	$b(nm)$	$a(nm)$
350	1.125	295.7	332.7
350	1.25	247.1	308.9
350	1.5	173.9	260.9
350	1.625	147.7	240.0
350	1.750	126.6	221.6
350	1.875	109.6	205.5

Table 2.2: Data used for the plot of the annihilation field as a function of the form factor f for the ellipses in fig. 2.7. Case of external field applied at 30°.

60° case			
$R_c(nm)$	f	$b(nm)$	$a(nm)$
300	1	300.0	300.0
300	1.05	302.4	317.5
300	1.1	302.2	332.4
300	1.15	299.6	344.5
300	1.2	294.7	353.6
300	1.25	287.9	359.9
300	1.3	279.5	363.4
300	1.35	269.9	364.4
300	1.4	259.3	363.0
300	1.45	248.1	359.7
300	1.5	236.5	354.8
300	1.625	207.4	337.0
300	1.750	179.9	314.8
300	1.875	155.4	291.4

Table 2.3: Data used for the plot of the annihilation field as a function of the form factor f for the ellipses in fig. 2.7. Case of external field applied at 60°.

So, some simulations were performed in order to demonstrate the validity of the formula obtained mathematically for ellipses and check if a generalization of Guslienko rigid vortex model is possible. The following graph shows the results (fig. 2.7) obtained for the annihilation field for different ellipses using the quantities showed in tables 2.2 and 2.3:

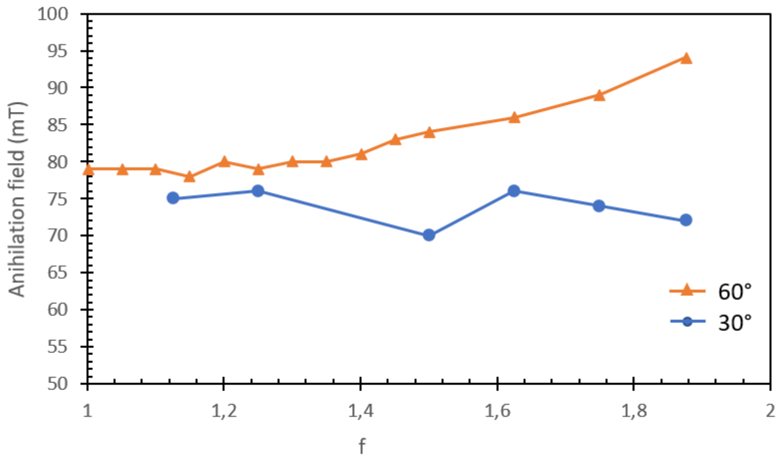

Figure 2.7: The graph shows the annihilation field as a function of the form factor, hence $f = a/b$. In particular there are two lines accounting for the two angles for which the ellipses were simulated, the blue circles are the results obtained for an external field applied at 30° with respect to the x axis (look fig. 2.6 for axis references), and orange triangles for an angles of 60°.

The results extrapolated from the graph are that for a fixed curvature's radius the annihilation field is the same independently from the other ellipses dimensions. To be more precise the rule seems to be valid only for the 30° case and for 60° for form factor smaller than 1.4. After that point, the curve behaves almost linearly.
A possible explanation to the results for 60° case it was found by studying the vortex core dynamics from the center to the edges.
A sequence of picture resulting from this study is shown (fig. 2.8):

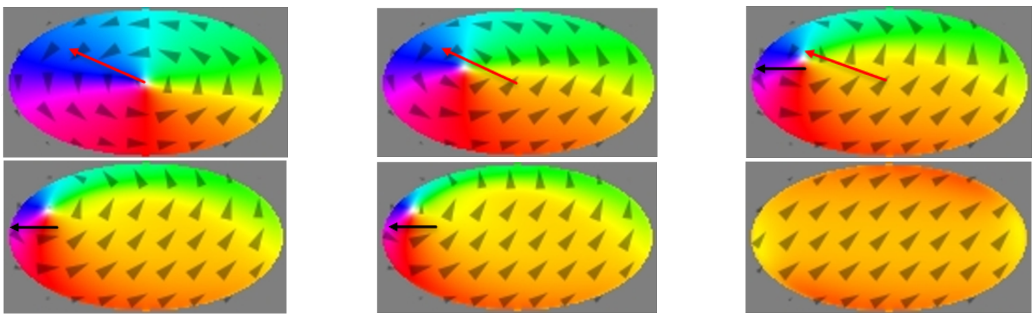

Figure 2.8: Simulation of the dynamic of a vortex while a field with an angle of 60° is applied (ordered from left to right and from top to bottom). The red arrow defines the expected track perpendicular with respect to the applied field. The black arrow defines the final track the core takes before to annihilate.

The vortex core motion follows the "expected track" only until a certain distance from the edges (look in sequence from left to right the three images of the first line of fig. 2.8). Then it will move horizontally until annihilation (sequence of the three images from left to right of the second line of fig. 2.8).
The "expected track" is defined by the relative angle Θ (see fig. 2.6 where it was already mentioned the link between vortex core motion and external applied field) with respect to the x axis. The explanation of the horizontal track rather than the expected, can be given by the asymmetrical effect of edges for high form factors.
The asymmetry is larger for angles close to the x axis (hence around $0°$ or $180°$). This asymmetry causes the vortex core to be forced to move in a not theorized direction, due to the lesser resistance with respect to the one of the expected track.

From a physical point of view, the point in the ellipse where it annihilates has a smaller curvature radius. In fact the curvature's radius is smaller for angles closer to the horizontal direction.
This leads to an annihilation field larger than expected, due to the inverse proportionality between annihilation field and curvature's radius.
Furthermore for the simulations performed, the curvature's radius along the horizontal direction is smaller for higher form factors (looking at the table 2.3 for higher form factors b is smaller, where b is also the radius of the largest in-circle in the ellipse). This justifies the linear dependence found for the annihilation field as a function of the form factor in the figure.

In conclusion, it is demonstrated for these results that for the ellipse the relation holds between the curvature's radius and the annihilation field. This confirm the purpose to generalize the formula presented by Guslienko [10] in the rigid vortex model, used to estimate the annihilation field in circular dots.
At the same time, this work demonstrate that it is possible to have a shape for the free layer of the MTJ able to enhance almost independently the susceptibility and the annihilation field.

2.3 Dot pair study and results

The other problem met during the study of circles with cut was the remanence magnetization. An analysis will be shown about the dot pairs interaction. The aim is to reduce the remanence, by studying different combinations of dot pairs having different interaction direction (along x or y) and cut position. Different simulations were performed. The results will give some hints in understanding if the interaction turns out to be useful or not to reduce magnetization remanence.

2.3.1 Results for dot pairs

Before discussing the results, it is important to give some explanations.
The study of dot pairs was performed for circular dots with a cut having the shape of a ring sector.

The reason why such a weird cut was performed lies in the easier description of the dot in polar coordinates. The objective was to check if numerical simulations would give the same results as an analytical description of the dot pair (based on the work of Sukhostavets et al. [19]).

First of all it is necessary to show the different configurations for the dot pairs simulated. The configurations are the following (fig. 2.9):

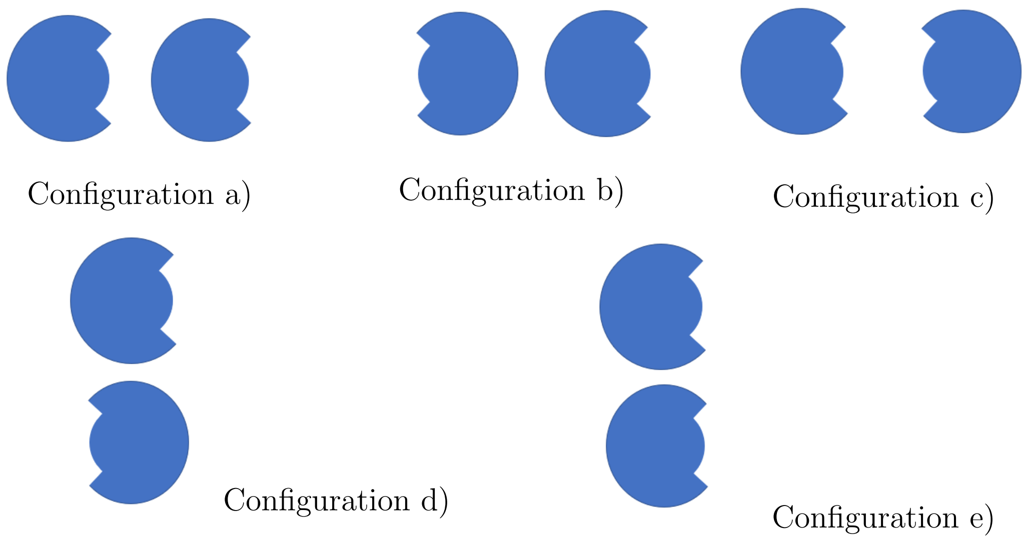

Figure 2.9: Circles aligned along x axis with cut on the same side (a), on opposite sides (b) and side by side (c); circles along y axis with cut on opposite sides (d) and on the same side (e).

In total 5 configurations were performed, in which 3 of them are interacting along the horizontal axis (top pictures) and 2 are interacting along the vertical axis (from now on they will be respectively defined as x and y axis).

Results of the simulations

Here the results for the ring sector shaped cut, in which each curve represents the behaviour of one configurations as a function of the distance between disk centers (normalized by the radius). (fig. 2.10):

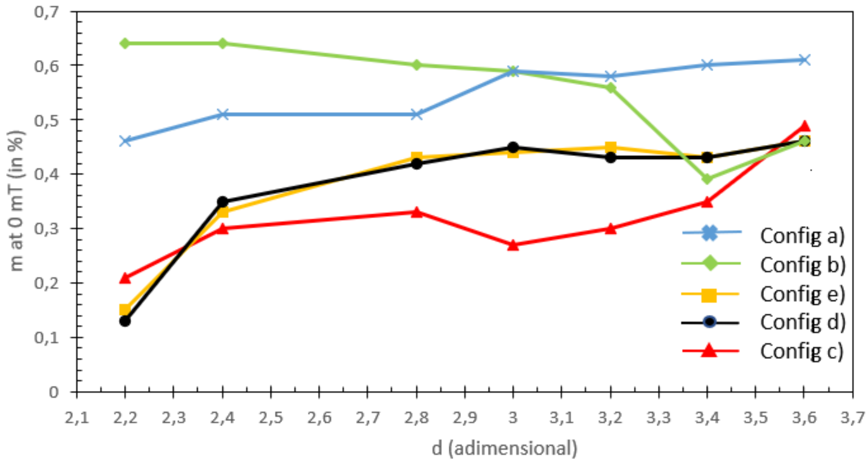

Figure 2.10: Simulations results' for the study of the dot pairs interaction for different dots' and cut's positions. m is the normalized magnetization defined as $m = \frac{M}{M_s}$, d the distance between disk centers normalized by the radius.

The picture show that among 5 configurations simulated, 3 of them shows a significant reduction of the remanence magnetization at zero external field (in particular c), d) and e) configurations).
It is a very interesting result, because it gives positive feedback about the idea to use dot pairs in order to reduce the remanence magnetization generated when working with MTJs having a flat.
Furthermore, it is always possible to play with parameters, by reducing the distance or increasing the radius of the dots and keeping a fixed distance between disk centers, to have at the end zero remanence magnetization. The reason lies in the definition of the factor used as x axis in the previous figure, being a normalized distance depending by the dots' radius.
This allow to perfectly fulfill the task for which the dot interaction was introduced at first.

2.4 Vortex core position for non-circular dots

In this section, a closer analysis of the vortex core position is shown to improve the understanding of the vortex state. In particular, the first part will give some hints about an analytical model developed by the research team. A mathematical description is given to understand the behaviour and the position of the vortex core in the presence of a cut. In the second part the aim is to verify such hypothesis, through micromagnetic simulations, and more generally to understand where the vortex core is placed.

2.4.1 Analytic model

The most important assumption considered is the validity of the RVM (rigid vortex model). When a vortex state nucleates in dots in the presence of a cut like a flat, the circular magnetization is maintained. But, as previously mentioned (in fig. 2.2), the vortex core is shifted with respect to the center of the original circle.
This leads to a reorganisation of the circular magnetization as shifted with respect to the center. To identify the real position of the vortex core after a cut is not straightforward. In fact it is necessary to take into account the energy factors of the new system and the relative residual magnetization.
The energy factors that play a role are the same as shown in Section 1.3.1, but they need to be adapted to this new disk shape. The formulas are not shown because they will introduce nothing of interest in the explanation of the phenomenon. Without going into further details, there are two alternative hypothesis at the moment:

- the vortex core is placed at geometrical barycenter
- the vortex core is placed at the center of the in-circle into the disk

The two points coincide with the circle center when there is no cut into the system. When instead a cut is introduced, they are shifted with respect to the center with two different values.

Here is a picture that can help understanding the position of the points in a real case for a disk with a flat (fig. 2.11):

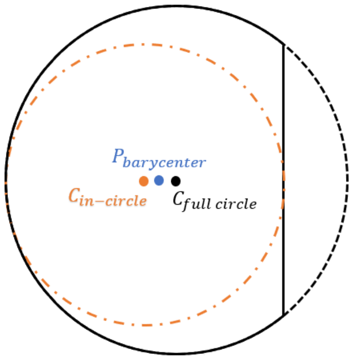

Figure 2.11: Illustration of the important points where to place the vortex core in a dot. In orange $C_{in-circle}$ is the center of the largest circle inscribed in the dot, in blue $P_{barycenter}$ is the resulting barycenter of the dot and in black $C_{fullcircle}$ is the center of the full circle without considering the cut.

The formula used to find the barycenter is the following:

$$x_G = \frac{\int_0^R 2yx dx}{\int_0^R 2y dx} \tag{2.4}$$

Here is a picture helping to understand the formula used to find the barycenter (fig. 2.12):

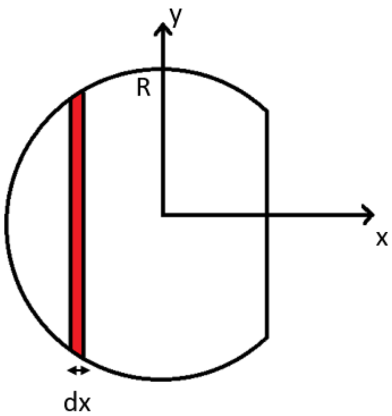

Figure 2.12: Illustration of the integral process in a dot with flat. The small area in red is a "small" rectangle in which the figure is ideally divided while integrating all over the space.

The dot is considered as made of a series of small rectangles spacing for all the x direction (like the red one in fig. 2.12). The dimensions of the rectangles are respectively: the local height y of the circle as first side, and an infinitesimal of the full length in x (dx). To find the barycenter, these rectangles are summed in an integral all over the disk shape.

Instead, the center of the largest in-circle can be easily defined by shifting the center of the full circle by the half of the penetration depth away from the cut. In this way, the position of the in-circle's center is exact in the case of the flat, while is approximated (but acceptable) for the ring sector missing shaped cut.

The study of the vortex core was performed for circular dots for two different types of cuts: the ring sector missing and the flat. In conclusion also some elliptical dots will be simulated and discussed due to the link with the circular dots but also because of their interesting properties. In fact it is possible to implement the use of a cut, as in the case of a circle, in order to control the circularity also in this case. In analogy to circles, it was also appreciated the presence of a remanence magnetization linked to the shift of the vortex core due to the introduction of an asymmetry (see fig. 2.13).

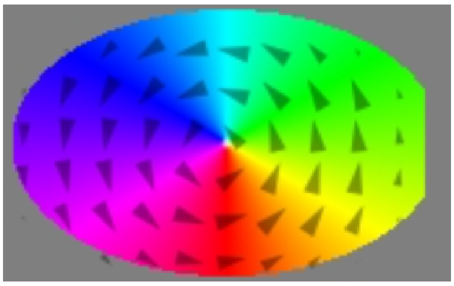

Figure 2.13: Figure showing a micromagnetic simulation's result of an ellipse with flat. The picture is taken for an external field equal to zero. The figure shows a counterclockwise circularity; it was obtained by increasing the field starting from negative annihilation field.

For ellipses it is possible to increase the distance between the two points considered as hypothesis. For example for a shallow flat, only the barycenter is shifted, while the center of the in-circle corresponds to the center of the ellipse.

Here is a picture that can help understanding the different point positions in an ellipse with a shallow flat (fig. 2.14):

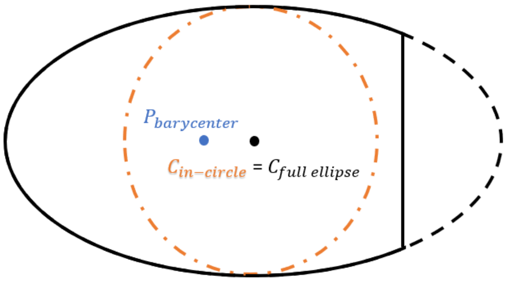

Figure 2.14: Illustration of the important points where to place the vortex core in an elliptic dot. In black $C_{in-circle}$ is the center of the largest circle inscribed in the dot that correspond also with $C_{fullellipse}$ that is the center of the full ellipse without considering the cut, in blue $P_{barycenter}$ is the resulting barycenter of the dot.

2.4.2 Micromagnetic simulations

To identify the vortex core position through simulations is not an easy task. There are no direct functions that are suited for this aim, this leads to push the program to its limits. At the end, the code implemented, gives just an idea of the vortex core position without giving exact results to be directly compared.

The idea behind the approach implemented can be found in the definition of the magnetic vortex state. In fact, the magnetization is in-plane for the majority of the dot volume except for the vortex core, where the magnetization is out-of-plane. Hence for the reference system used in this work, the out-of-plane magnetization is directed along the z-axis.
Since the vortex core is the center for the circular in-plane magnetization, it is important to identify its position in order to understand the magnetic behaviour of the system. In particular, it could be useful to look for the value of the out-of-plane magnetization in the dot.
An higher m_z amplitude should be associated with the identification of the vortex core position. It is important to remind from literature that, the vortex core is approximately $10 - 20\ nm$ large[17].

Furthermore, the vortex core position identifies a point where the in-plane magnetization passes from positive to negative for each axis. In fact this is the point where the magnetic configuration shows a switch in the direction of the majority of the magnetic moments, passing from up to down (or vice versa) with respect to the y-axis (as illustrated in fig 2.15):

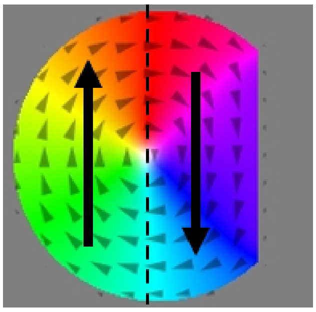

Figure 2.15: Illustration of the main resulting magnetization at the different sides of the vortex core position.

This is the reason why the in-plane magnetization results will also be shown. In fact, the vortex core position can be roughly determined when a switch of the magnetization is observed (in the Y or X-axis).

The basic idea was to consider different regions for the disk and look for the local magnetization along the z direction (m_z out-of-plane magnetization) to identify the position where the vortex core lies.
As a support to this result the in-plane magnetization was also studied for each region, for the reasons explained earlier. Here is an illustration of the definition of the regions in one of the disks simulated (fig. 2.16):

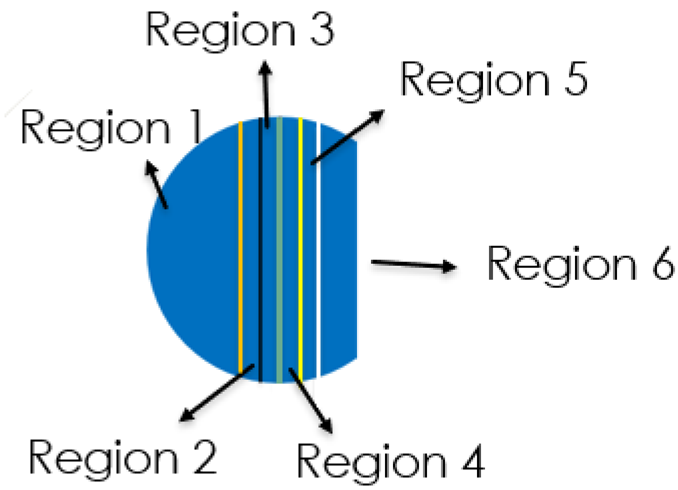

Figure 2.16: Disk simulated for the study of the vortex core position, 6 regions are defined around a given point (the green line in the figure), that can be either the barycenter or the in-circle's center. The radius is $125nm$, the other lines are $6nm$ away one from each other.

The idea at the beginning was to place small regions, to the left and to the right of a given point. The given point in accordance with the two ideas mentioned before, in one simulation is the center of the in-circle, in the other case, is the geometrical barycenter found through the resolution of the eq. 2.4. After some trials, it merged that the optimal way to perform the simulation was by placing several regions around the hypothetical point, more specifically 3 to the right and 3 to the left.

Furthermore these regions are also placed in an inner part of the free layer and not its total thickness. In fact while studying the out of plane magnetization for a full layer, it appeared that probably the effects of the external surfaces can bend the magnetization found along z, giving at the end, wrong results.
Here is a representation of the part of layer studied (in fig. 2.17):

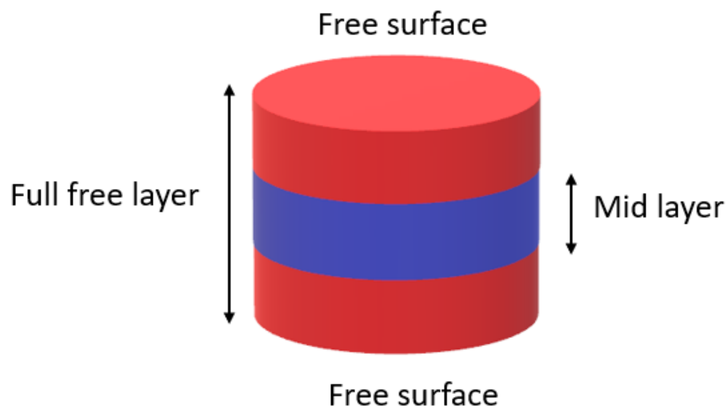

Figure 2.17: Drawing showing the part of the free layer considered while simulating in order to remove artifacts caused by the surfaces.

Circular dots

Before showing the results it is necessary to give the geometry dimensions: the radius of the circular dot is $R = 125nm$, the thickness is $33nm$ but the layer studied is only $12nm$ (see 2.17), for the reasons explained earlier. The penetration factors are respectively $p = 30\%$ of the radius for the flat and $p = 15\%$ for the ring sector. With these quantities the barycenter evaluated for the circle with a flat is $x_{G,F} = -10.3nm$ while for the ring sector is $x_{G,RS} = -7.8nm$. While the in-circle's centers are $x_{ic,F} = -18nm$ and $x_{ic,RS} = -9nm$.

It is necessary to say that all the simulations were performed with a cut placed at the right of the disk (as in fig 2.16). The nucleation process was performed with decreasing positive external applied fields along the vertical direction. This allows to say that the circularity for the simulations will always be clockwise.
The position of the lines showed in fig. 2.16 for the barycenter are (tab. 2.4):

values in nanometers (nm)					
	line 1	line 2	Barycenter	line 3	line 4
RING SECTOR	-19.8	-13.8	**-7.8**	-1.8	4.2
FLAT	-22.3	-16.3	**-10.3**	-4.3	1.7

Table 2.4: Lines position connected to the ones showed in fig. 2.16 for the barycenter. The first line separates region 1 and 2, the second line separates region 2 and 3 and so on.

While for the in-circle's center, the positions are the following (tab. 2.5):

values in nanometers (nm)					
	line 1	line 2	In-circle's center	line 3	line 4
RING SECTOR	-21	-15	**-9**	-3	3
FLAT	-30	-24	**-18**	-12	-6

Table 2.5: Lines position connected to the ones showed in fig. 2.16 for the in-circle's center. The first line separates region 1 and 2, the second line separates region 2 and 3 and so on.

First of all, the resulting global magnetization of the dot is showed when considering only the inner layer as defined in fig. 2.17 (tab. 2.6):

This information is useful because it tells in which direction the vortex core is shifted with respect to the theoretical position at zero remanence for a given circularity. In

	m at 0 mT	m at 0 mT (in %)
RING SECT	0.005200728	0.52 %
FLAT	-0.005887522	-0.59 %

Table 2.6: Remanence magnetization for the two circles simulated, one with a flat and the other with the shape of a ring sector.

fact later, the theoretical position for the vortex core considered is the one for the case of no residual in-plane magnetization.

Something important is the sign of the remanence that changes for the same circle when looking to one cut or the other.

Here showed the magnetization values found. The tables 2.7, 2.8 show respectively the magnetization out and in-plane for the different regions around the barycenter:

m_z out of plane magnetization (circular dot)						
	region 1	region 2	region 3	region 4	region 5	region 6
RING SECTOR	-0.00466	0.04530	**0.07569**	**0.07390**	0.04213	-0.00480
FLAT	-0.00383	**0.06184**	**0.08378**	**0.06415**	0.02722	-0.00575

Table 2.7: Out of plane magnetization for the two types of circle simulated taking into account the six regions in which the simulation was divided. The regions are defined with respect to the barycenter.

m_y in plane magnetization (circular dot)						
	region 1	region 2	region 3	region 4	region 5	region 6
RING SECTOR	0.71399	0.26556	**0.11503**	**-0.0598**	-0.21204	-0.69830
FLAT	0.71177	0.24086	**0.0723**	**-0.1034**	-0.24330	-0.70838

Table 2.8: In-plane magnetization for the two types of circle simulated taking into account the six regions in which the simulation was divided. The regions are defined with respect to the barycenter.

The bold values in the tables shown are used to identify the hypothetical regions where the vortex core is placed.

Instead the following two tables 2.9, 2.10 show again the magnetization out and in-plane in the hypothesis for the different regions around the incircle's center:

m_z out of plane magnetization (circular dot)						
	region 1	region 2	region 3	region 4	region 5	region 6
RING SECTOR	-0.00520	0.00364	**0.07013**	**0.07808**	0.05113	-0.00419
FLAT	-0.00658	0.01778	0.05273	**0.0818**	**0.07229**	-0.00244

Table 2.9: Out of plane magnetization for the two types of circle simulated taking into account the six regions in which the simulation was divided. The regions are defined with respect to the incircle's center.

m_y in plane magnetization (circular dot)						
	region 1	region 2	region 3	region 4	region 5	region 6
RING SECTOR	0.72117	0.29606	**0.15665**	**-0.0165**	-0.17779	-0.69026
FLAT	0.74735	0.39041	0.27641	**0.11755**	**-0.0622**	-0.66604

Table 2.10: In plane magnetization for the two types of circle simulated taking into account the four regions in which the simulation was divided.The regions are defined with respect to the incircle's center.

RING SECTOR CASE: By combining the results obtained within the two different hypothesis for m_y and m_z, it is possible to say that the ideal vortex core position for no remanence magnetization is found between $[-13.8nm; -7.8nm]$. This result already takes into account the positive global magnetization (tab. 2.6), that gives (from simulations) a vortex core shifted to the right with respect to its ideal position. The given considerations are obtained by looking into the tables at the bolded values and by intersecting the region results for the four tables.

FLAT CASE: By combining the results obtained in the two different hypothesis for m_y and m_z, it is possible to say that the ideal vortex core position is identified between $[-16.3nm; -6nm]$. This result already takes into account the negative global magnetization (tab. 2.6), that gives (from simulations) a vortex core shifted to the left with respect to its ideal position.
The result is extrapolated in the same way of the ring sector case.

Elliptical dots

The same type of study and relative simulations were performed for the ellipse. The reason why also ellipses are included in the study is for the ability to distinguish better than with circles the barycenter and the incircle's center positions. The dimensions of the ellipse simulated are: $b = 125nm$, $f = 1.7$ (hence $a = 212.5nm$), a penetration factor of the 30%. The evaluation of the barycenter is the same as for the case for circles, based on the equation (2.2). The value found was $x_G = -17nm$, while for this ellipse the center of the in-circle is placed at the center of the full ellipse $x_{ic} = 0nm$ due to the small penetration that doesn't shift the biggest in-circle from full ellipse's center (see also fig. 2.14).

Again it is important at first to show the global magnetization to understand the direction of the shift of the vortex core position of the simulation with respect to the point where no residual magnetization is appreciated (tab. 2.11)

	m at 0 mT	m at 0 mT (in %)
FLAT	0.00242054	0.24 %

Table 2.11: Remanence magnetization for the ellipse simulated

Here the tables resuming the results obtained for the ellipse (tabb. 2.12, 2.13):

m_z out of plane magnetization (ellipse)						
	region 1	region 2	region 3	region 4	region 5	region 6
CENTER	0.00082	**-0.0611**	**-0.0679**	**-0.0533**	-0.02853	-0.00284
BARYCENTER	0.00320	-0.00194	**-0.0205**	**-0.0448**	**-0.0648**	-0.00237

Table 2.12: Out of plane magnetization for the two possible definition of the six regions (either with respect to the ellipse center or the barycenter) in which the simulation was divided.

m_y in plane magnetization (ellipse)						
	region 1	region 2	region 3	region 4	region 5	region 6
CENTER	0.60420	**0.09190**	**-0.0168**	-0.12122	-0.20561	-0.63677
BARYCENTER	0.64633	0.29961	0.24114	0.16364	**0.06558**	**-0.5848**

Table 2.13: Out of plane magnetization for the two definitions of the six regions in which the simulation was divided.

By combining the results obtained in the two different hypothesis for m_y and m_z, it is possible to say that the ideal vortex core position (the point that gives zero remanence) is found between $[-11nm; -5nm]$. This result already takes into account the positive global magnetization (tab. 2.6), that gives (from simulations) a vortex core shifted to the right with respect to its ideal position.
Here the conclusions about the vortex core position are given by looking to the bolded values in the table and intersecting the relative position for each result.

2.4.3 Analysis of the results

The position of the vortex core was identified.
Unfortunately for the ring sector, the interval include both points considered in the initial hypothesis. While for the flat case, the region where it is possible to find the vortex core exclude the in-circle's center.
This allows to conclude that the idea to consider the vortex core placed at the in-circle's center is wrong. At the same time, the other hypothesis will also give an approximation of the real position.
As a confirmation, the ellipse results exclude the vortex core to be placed at the barycenter, but it is not even found at the center of the ellipse.
The only conclusion is that another model need to be implemented. In particular, a possible idea is to consider the vortex core placed at the magnetization averaged barycenter. Unfortunately, this work is still in progress. It will be explored in the future with a PhD.

In the end, the chapter showed all the results obtained through micromagnetic simulations on all the subjects. The results of simulations show that the vortex state is an interesting magnetic configuration. It is possible to have a natural linear response, suited for applications like sensors or memories; furthermore, the drawbacks found with the first simulations like the control of nucleation were also solved. Furthermore, the chapter includes also the study of elliptical geometries and couples of dots that gave important results and they optimized the firsts simulations of the isolated circular dots. Finally, an analysis of the vortex core position was done, but it turned out that this question requires further analysis.

Conclusions

In this internship, it was studied the behaviour of magnetic vortex state based MTJs. They were also studied different geometries of the free layer and their effect on the vortex characteristics (mainly annihilation field, susceptibility, magnetization at remanence). The analysis started with the study of circular dots (as it's the usually chosen geometry). This geometry has some drawbacks like the unpredictability of the circularity after nucleation and the inverse proportionality between susceptibility and annihilation field.

The study of circles with flat gave the possibility to control the circularity at the expense of a remanence magnetization.

With the study of the elliptically shaped dots, a solution to the trade-off between nucleation field and susceptibility was found which allowed the introduction of a new degree of freedom in MTJs.

The study of dot pairs interaction showed the possibility to reduce the remanence magnetization, in order to solve the drawback due to the use of a flat.

The study of the vortex core position gave as a results that the models developped are not detailed enough to give an exact evaluation of its position. A new and possibly more accurate model was proposed. The identification of the exact position of the vortex core can help in the evaluation of an analytical value for the remanence magnetization to be compared with the simulation results.

In conclusion, the work explored many problems related to MTJs with a vortex state. If for some of them, the results given are complete and exhaustive, having solved all the problems found. For others, further studies are necessary. In fact a lot of phenomena still need to be studied more to understand the details of this particular state.

For this reason, due to the magnitude of work still to be explored, a future PhD thesis based on MTJs with a vortex state would be a natural continuation of the internship carried out in the last six month of the Master degree.

Bibliography

1. M. N. Baibich. J. M. Broto, A. Fert, F. Nguyen Vandau, F. Petroff, P. Etienne, G. Creuzet. A. Frederick and J. Chatelas, *"Giant Magnetoresistance of (001)Fe/(001)Cr magnetic superlattices"*, Physics Review Letters, Vol. 61 no. 21, p. 2472 (1988).

2. G. Binasch, P. Grunberg, F. Saurenbach, W. Zinn, *"Enhanced Magnetoresistance In Layered Magnetic-Structures With Antiferromagnetic Interlayer Exchange"*. Physical Review B. 39(7), pp. 4828–4830 (1989).

3. M. Julliére, *"Tunneling between ferromagnetic films"*, Physics Letters, Vol. 54A n.3, pp. 225-226 (1975).

4. M. Hosomi, H. Yamagishi, T. Yamamoto, K. Bessho, Y. Higo, K. Yamane, H. Yamada, M. Shoji, H. Hachino, C. Fukumoto, H. Nagao, and H. Kano, *"A Novel Nonvolatile Memory with Spin Torque Transfer Magnetization Switching: Spin-RAM"*, IEEE International Electron Devices Meeting, 2005. IEDM Tech Dig., Washington, DC, 2005, pp. 459-462.

5. J. P. Valadeiro, J. Amaral, Diana C. Leitão, R. Ferreira, S. F. Cardoso, and Paulo J. P. Freitas, *"Strategies for pTesla Field Detection Using Magnetoresistive Sensors With a Soft Pinned Sensing Layer"*, IEEE transactions on magnetics, Vol. 51 no. 1, 4400204 (2015).

6. K. Yu. Guslienko, *"Magnetic Vortex State Stability, Reversal and Dynamics in Restricted Geometries"*. Journal of Nanoscience and Nanotechnology Vol.8, 2745–2760 pp. 2749-2750 (2008).

7. K. Yu. Guslienko, V. Novosad, Y. Otani, *"Magnetization reversal due to vortex nucleation,displacement and annihilation in submicron ferromagnetic dot arrays"*. Physical review B., Vol. 65 p. 024414-6 (2002).

8. J. A. J. Burgess, J. E. Losby, M. R. Freeman, *"An analytical model for vortex core pinning in a micromagnetic disk"*. Journal of Magnetism and Magnetic Materials, Vol. 361 pp. 141-145 (2014).

9. S. Agramunt-Puig, N. Del-Valle, C. Navau, A. Sanchez, *"Controlling vortex chirality and polarity by geometry in magnetic nanodots"*. Applied Physics Letters, Vol. 104, p. 012407 (2014).

10. K. Yu. Guslienko, V. Novosad, Y. Otani, *"Magnetization reversal due to vortex nucleation, displacement and annihilation in submicron ferromagnetic dot arrays"*. Physical review B., Vol.65 p. 024414-3 (2002).

11. N.Usov et S.E.Peschannyj, *"Vortex distribution of magnetization in thin ferromagnetic cylinder"*. Fizika Metallov i Metallovedenie, Vol. 78, pp. 13-24, (1994).

12. A. Vansteenkiste, J. Leliaert, M. Dvornik, M. Helsen, F. Garcia-Sanchez and B. Van Waeyenberge, *"The design and verification of mumax3"*. AIP Advances 4, Vol. 4, 107133 (2014).

13. C. Reig, S. Cardoso de Freitas, S. C. Mukhopadhyay, *"Giant Magnetoresistance (GMR) Sensors: from basis to state-of-the-art applications"*, Springer 1^{st} Edition, Chapter 1 (2013).

14. O. Fruchart, *"LECTURE NOTES ON Nanomagnetism"*, pp 144-145 `http://fruchart.eu.`

15. K. Tsunekawa, D. D. Djayaprawira, M. Nagai, H. Maehara, S. Yamagata, N. Watanabe, S. Yuasa, Y. Suzuki, K. Ando, *"Giant tunneling magnetoresistance effect in low-resistance $CoFeB/MgO(001)/CoFeB$ magnetic tunnel junctions for read-head applications"*. Applied Physics Letters, Vol 87 no. 7, p. 072503-1 (2005).

16. K. Tsunekawa, D. D. Djayaprawira, M. Nagai, H. Maehara, S. Yamagata, N. Watanabe, S. Yuasa, Y. Suzuki, K. Ando, *"230% room-temperature magnetoresistance in $CoFeB/MgO/CoFeB$ magnetic tunnel junctions"*. Applied Physics Letters, Vol 86 no. 9, p. 092502-1 (2005).

17. M. Goiriena-Goikoetxea, K. Y. Guslienko, M. Rouco, I. Orue, E. Berganza, M. Jaafar, A. Asenjo, M. L. Fernández-Gubieda, L. Fernández Barquíng and A. García-Arribas, *"Magnetization reversal in circular vortex dots of small radius"*. Nanoscale, Vol. 9 , p. 11270 (2017).

18. M. Rahm, M. Schneider, J. Biberger, R. Pulwey, J. Zweck, and D. Weiss, *"Vortex nucleation in submicrometer ferromagnetic disks"*. Applied Physics Letters, Vol. 82 no. 23, pp. 4110-4112 (2003).

19. O. V. Sukhostavets, J. Gonzalez, and K. Y. Guslienko, *"Multipole magnetostatic interactions and collective vortex excitations in dot pairs, chains, and*

two-dimensional arrays". Physical review B., Vol.82, 094402 (2013).

20. K. L. Metlov, K. Y. Guslienko, *"Stability of magnetic vortex in soft magnetic nano-sized circular cylinder"*. Journal of Magnetism and Magnetic Materials, Vol. 242-245, pp 1015-1017 (2002).
21. K. Y. Guslienko, *"Magnetic vortex state stability reversal and dynamics in restricted geometries"*. Journal of Nanoscience and Nanotechnology, Vol. 8 no. 6, pp. 2745-2760 (2008).
22. H. Cai, W. Kang, Y. Wang, L. Naviner, J. Yang, W. Zhao, *"High Performance MRAM with Spin-Transfer-Torque and Voltage-Controlled Magnetic Anisotropy Effects"*. Applied sciences Vol.7, p. 929 (2017).
23. I.N. Bronstein and K.A. Semendiaev, "aide-mémoire de mathématiques", Ed. Eyrolles (Paris, 1985)

Appendix

Curvature radius

The definition of the curvature radius is taken from literature [23]. The formula is the following (eq. 2.5):

$$R_c(x_0, y_0) = a^2 b^2 \left(\frac{x_0^4}{a^2} + \frac{y_0^4}{b^2}\right)^{\frac{3}{2}} \tag{2.5}$$

where a and b are respectively the semi-major and semi-minor axis of the ellipse, and x_0 and y_0 are the coordinates of a random point of the ellipse where the curvature's radius is evaluated.

It is possible to find the curvature for each point of the ellipse perimeter by solving the following system of equations:

$$\begin{cases} y = \tan(\theta)x \\ \frac{x^2}{a^2} + \frac{y^2}{b^2} = 1 \end{cases}$$

where θ is the angle for the straight line with respect to the x-axis.
Here is a picture that graphically shows the two equations of the system (fig. 2.18):

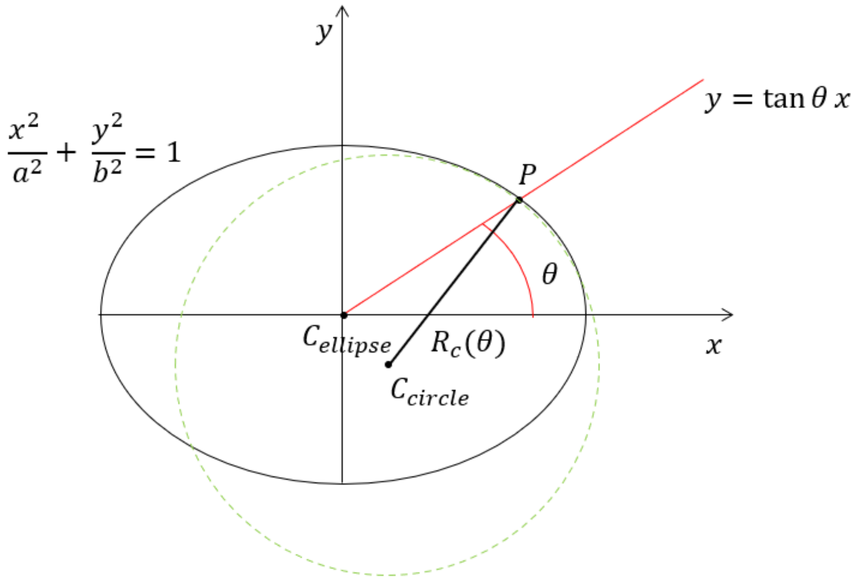

Figure 2.18: Graphic illustrations of the two equations of the system used to find the curvature's radius for generic angles θ. P is the common point between the straight line and the ellipse, R_c is the curvature radius evaluated in that point for a circle that approximate the circular behaviour of the ellipse in P.

Going back to the demonstration, By substituting the first equation of the system into the second, the following equation is obtained (eq. 2.6):

$$\frac{x^2}{a^2} + \frac{x^2 \tan(\theta)^2}{b^2} = 1 \tag{2.6}$$

The final scope is to find from this equation the x coordinate as a function of a, b and θ (eq. 2.7):

$$\frac{b^2x^2 + a^2b^2 \tan(\theta)^2}{a^2b^2} = \frac{a^2b^2}{a^2b^2} \tag{2.7}$$

$$x^2\left(b^2 + a^2 \tan(\theta)^2\right) = a^2b^2 \tag{2.8}$$

$$x^2 = \frac{a^2b^2}{b^2 + a^2 \tan(\theta)^2} \tag{2.9}$$

$$x = \pm \frac{ab}{\sqrt{b^2 + a^2 \tan(\theta)^2}} \tag{2.10}$$

where only the positive solution is taken into account.

Substituting the x coordinate found in one of the two equations of the system, also the y coordinate is found. For simplicity of calculations, the first equation of the system will be used (eq. 2.11):

$$y = \frac{ab\tan(\theta)}{\sqrt{b^2 + a^2 \tan(\theta)^2}} \tag{2.11}$$

In this demonstration x and y correspond with the coordinates x_0, y_0. Now it is possible to insert them in the definition for the curvature radius (eq. 2.5) obtaining (eq. 2.12):

$$R_c = a^2b^2\Big(\frac{a^2b^2}{a^4(b^2 + a^2\tan^2(\theta))} + \frac{a^2b^2\tan^2(\theta)}{b^4(b^2 + a^2\tan^2(\theta))}\Big)^{\frac{3}{2}} \tag{2.12}$$

$$R_c = a^2b^2\Big(\frac{\frac{b^2}{a^2} + \frac{a^2\tan(\theta)^2}{b^2}}{b^2 + a^2\tan(\theta)^2}\Big)^{\frac{3}{2}} \tag{2.13}$$

The eq. 2.13 can be written in a more compacted form by collecting both at the numerator and the denominator the quantity b^2/a^2, and collecting a^2 at the denominator (eq 2.14):

$$R_c = \frac{b^2}{a}\Big(\frac{1 + \frac{a^4\tan(\theta)^2}{b^4}}{1 + \frac{a^2}{b^2}\tan(\theta)^2}\Big)^{\frac{3}{2}} \tag{2.14}$$

But as already mentioned a/b is the form factor f. In conclusion, the resulting formula is the following (eq. 2.15):

$$R_c = \frac{b}{f}\Big(\frac{1 + f^4\tan(\theta)^2}{1 + f^2\tan(\theta)^2}\Big)^{\frac{3}{2}} \tag{2.15}$$

Being the same equation showed in section 2.2.2 (eq. 2.3) and the one used for the calculations implemented during the work.

Barycenter

Starting from the equation shown in section 2.4.1 (eq 2.4), it is possible to adapt it to a given geometry in order to find an analytical formula for the barycenter.
In this case it was used for 3 different dots: a circle with a flat, a circle with a ring sector missing and an ellipse with a flat.
For computational simplicity, each dot will be divided in two parts, one left and one right with respect to the center of the full circle (or ellipse) as it will be shown in each section. The complete barycenters evaluation it will be shown in the following pages for all the dots simulated in this work.

Circle with flat

Here is a picture showing the flat modelisation used (fig. 2.19):

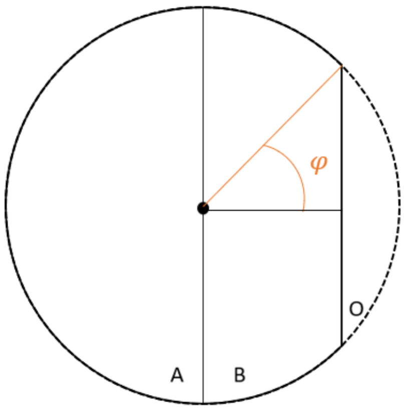

Figure 2.19: Graphic illustrations of the two regions defined for a circle with flat. Three regions are defined A, B and O (for the removed part). The orange arc represent the angle φ related to the cut dimension.

In the case of the circle with a flat, the barycenter of the region A is easily evaluated by substituting to the barycenter formula (eq. 2.4) the polar coordinates: $y = R\sin(\theta)$, $x = R\cos(\theta)$, $dx = -R\sin(\theta)d\theta$, obtaining (eq. 2.16):

$$x_{G,A} = \frac{-R^3 \int_0^{\pi/2} \sin^2(\theta)\cos\theta d\theta}{R^2 \int_0^{\pi/2} \sin^2(\theta) d\theta} \tag{2.16}$$

$$x_{G,A} = \frac{\frac{-R^3}{3}[sin^3(\theta)]_0^{\pi/2}}{R^2[\frac{\theta}{2} - \frac{\sin^2(\theta)}{4}]_0^{\pi/2}} \tag{2.17}$$

Resulting to the well-known formula for the barycenter of half circle (eq. 2.18):

$$x_{G,A} = -\frac{4R}{3\pi} \tag{2.18}$$

The barycenter for region B is instead (eq. 2.19):

$$x_{G,B} = \frac{-R^3 \int_{\pi/2}^{\varphi} \sin^2(\theta) \cos\theta d\theta}{R^2 \int_{\pi/2}^{\varphi} \sin^2(\theta) d\theta} \tag{2.19}$$

$$x_{G,B} = \frac{-R^3/3[sin^3(\theta)]_{\pi/2}^{\varphi}}{R^2[\frac{\theta}{2} - \frac{\sin^2(\theta)}{4}]_{\pi/2}^{\varphi}} \tag{2.20}$$

$$x_{G,B} = \frac{\frac{2R^3}{3}[1 - \sin^3(\varphi)]}{\frac{\pi}{2} - \varphi + \frac{sin(2\varphi)}{2}} \tag{2.21}$$

For the evaluation of the total barycenter it is also necessary to have the surfaces of the two regions that are (eq 2.22):

$$S_A = \frac{\pi R^2}{2} \tag{2.22}$$

for the half circle (region A), and (eq. 2.23):

$$S_B = R^2\Big(\frac{\pi}{2} - \varphi + \frac{sin^3(\varphi)}{2}\Big) \tag{2.23}$$

for the half circle with cut (region B).

In conclusion the total barycenter can be found by averaging the partial barycenters. The formula is (eq. 2.24):

$$x_G = \frac{x_{G,A}S_A + x_{G,B}S_B}{S_A + S_B} \tag{2.24}$$

The equation obtained at the end when substituting is (eq. 2.25):

$$x_G = -\frac{2}{3}R\frac{\sin^3(\varphi)}{\pi - \varphi + \frac{\sin(2\varphi)}{2}} \tag{2.25}$$

Circle with ring sector missing

Here is a picture of the modelisation used for the circle with a ring sector missing (fig. 2.20):

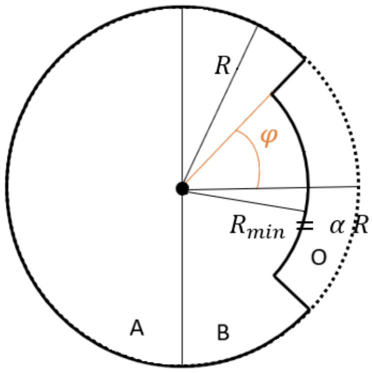

Figure 2.20: Graphic illustrations of the two regions in which this dot is divided. R_{min} is the radius for the smaller circle of the system. The orange arc represents the angle φ related to the cut dimensions.

As in the previous section, the results obtained for the region A are the same being in both cases half circle, hence they are already know the $x_{G,A}$ (eq. 2.18) and the surface S_A (eq. 2.22).

While for region B, new calculations are required.
The definition of the barycenter is the same (eq. 2.4), but in this case for a particular shape. The idea is to evaluate the barycenter of half circle and then remove the baricenter for a part of a ring sector (from fig. 2.20 region B is like region A subtracting the region O). With this approach, the barycenter of region B can be written as (eq. 2.26):

$$x_{G,B} = \frac{\int_0^R 2yxdx - \int_{\alpha R}^R 2yxdx}{\int_0^R 2ydx} \tag{2.26}$$

where the second integral at the numerator is the baricenter of the region O to be removed. αR is the radius of the smaller circle (also called R_{min}), that defines the part of ring sector removed (see fig. 2.20).

Solving the integral, the following equation is obtained (eq. 2.27):

$$x_{G,B} = \frac{\frac{2R^3}{3} - \frac{2\sin(\varphi)}{3\varphi\frac{R^2+R_{min}^2+RR_{min}}{R+R_{min}}}\frac{\pi\varphi}{180}(R^2 - R_{min}^2)}{\frac{\pi R^2}{2} - \frac{\pi\varphi}{180}(R^2 - R_{min}^2)} \tag{2.27}$$

The formula obtained is long and complicated, but it is possible to simplify it. In particular at the end the formula for the dot barycenter is obtained in the same way of the previous section (eq. 2.24) obtaining (eq. 2.28):

$$x_G = -\frac{2R}{3}\frac{\sin(\varphi)(1-\alpha^3)}{\pi - \varphi(1-\alpha^2)} \tag{2.28}$$

Ellipse with flat

Also for the ellipse the modelisation is similar, based on eq. 2.4 with some adaptations and with the definition of two regions as follows (fig. 2.21):

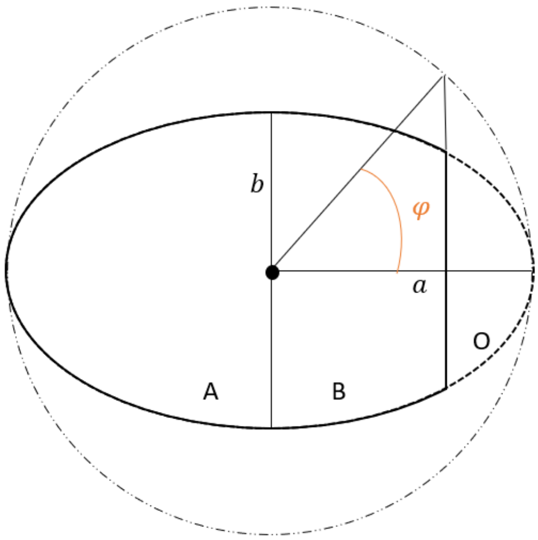

Figure 2.21: Graphic illustrations of the two regions defined for an ellipse with a flat. The orange arc represents the angle φ related to the cut dimension.

One important remark need to be done about the angle in this case. In fact differently from the case of the circle, here the angle associated to the cut is defined respect to the circle with radius equal to the semi-major axis of the ellipse. In this way it is possible to have a value for the barycenter that has a similar structure of the results found for the circle.

For the region A, the equation is defined as (eq. 2.29):

$$x_{G,A} = \frac{\int_{-a}^{0} 2yxdx}{\int_{-a}^{0} 2ydx} \tag{2.29}$$

$$x_{G,A} = \frac{-2a^2b\int_{\pi}^{\pi/2} \sin^2(\theta)\cos\theta d\theta}{-2ab\int_{\pi}^{\pi/2} \sin^2(\theta)d\theta} \tag{2.30}$$

$$x_{G,A} = \frac{\frac{a}{3}[sin^3(\theta)]_{\pi}^{\pi/2}}{[\frac{\theta}{2} - \frac{\sin(2\theta)}{4}]_{\pi}^{\pi/2}} \tag{2.31}$$

Resulting to the well-known formula for the barycenter of half ellipse (eq. 2.32):

$$x_{G,A} = -\frac{4a}{3\pi} \tag{2.32}$$

With similar considerations, for the region B it is possible to write (eq. 2.33):

$$x_{G,B} = \frac{-2a^2b\int_{\pi/2}^{\varphi} \sin^2(\theta)\cos\theta d\theta}{-2ab\int_{\pi/2}^{\varphi} \sin^2(\theta)d\theta} \tag{2.33}$$

$$x_{G,B} = \frac{a/3[sin^3(\theta)]_{\pi/2}^{\varphi}}{1/2[\frac{\theta}{2} - \frac{\sin(2\theta)}{4}]_{\pi/2}^{\varphi}} \tag{2.34}$$

$$x_{G,B} = \frac{\frac{2a}{3}[1 - \sin^3(\varphi)]}{\frac{\pi}{2} - \varphi + \frac{sin(2\varphi)}{2}} \tag{2.35}$$

The surfaces instead are (eq. 2.36 and 2.37):

$$S_A = \frac{\pi ab}{2} \tag{2.36}$$

$$S_B = ab(\frac{\pi}{2} - \varphi + \frac{sin(2\varphi)}{2}) \tag{2.37}$$

As in the case of circular dots, the total barycenter is obtained from eq. 2.24, resulting in (eq. 2.38):

$$x_G = -\frac{2a}{3}\frac{sin^3(\varphi)}{\pi - \varphi + \frac{\sin(2\varphi)}{2}} \tag{2.38}$$

The equations 2.25, 2.28 and 2.38 were used in the section 2.4.1 to evaluate the barycenter for the relative regions.

Résumé

Le présent rapport offre une vision de l'état magnétique de vortex. Notamment l'étude les phénomènes physiques spécifiques de cet état rencontré lors des simulations effectuées sur un matériau magnétique de forme circulaire et leur application dans les jonction à effet tunnel magnétique.
Les thèmes traités par ces travaux varient entre l'identification des champs magnétiques de renversement associée au présence d'un état magnetique de vortex, et l'étude des effets de géométries particulières comme le meplat ou l'ellipse sur le comportement de l'état magnétique.
Ce travail montre que certaines réprésentations géométriques (par exemple l'ellipse) ont des avantages physiques et sont preferable lors de la génération d'un état magnétique de vortex dans la couche de détection d'une jonction à effet tunnel magnétique.

Abstract

This report gives an outlook to the vortex magnetic state, in particular the study of its typical physical phenomena, met while simulating a circular shaped magnetic material and its applications into MTJs (magnetic tunnel junctions).
The subjects covered by this document range from the identification of the magnetic field interval of the vortex state, to the study of particular geometries like circles with flat or ellipses.
This work demonstrates that some geometries (like the ellipse) have physical advantages and have to be preferred when generating a vortex state into the sense layer of a MTJ (magnetic tunnel junction).